MNRAS **000**, 1–27 (2018) Preprint 12 July 2022 Compiled using MNRAS LATEX style file v3.0

Virial masses of late type galaxies from the SDSS DR16

A. Nigoche-Netro[1⋆], E. de la Fuente[2,3∗], R. J. Diaz[4,5], M. P. Agüero[5,6], S. N. Kemp[1], R. A. Marquez-Lugo[1], P. Lagos[7], A. Ruelas-Mayorga[8], N. L. López-Contreras[1]

[1] *Instituto de Astronomía y Meteorología, CUCEI, Universidad de Guadalajara, Guadalajara, Jal. 44130, México.*
[2] *Departamento de Física, CUCEI, Universidad de Guadalajara, Guadalajara, Jal. 44130, México.*
[3] *Institute for Cosmic Ray Research, University of Tokyo, Kashiwanoha campus, Chiba, Japan (Sabbatical 2021).*
[4] *Gemini Observatory, NSF's NOIRLab, 950 N Cherry Ave, Tucson AZ, USA.*
[5] *Universidad Nacional de Córdoba, Laprida 854, Córdoba, CPA: X5000BGR, Argentina.*
[6] *Consejo Nacional de Investigaciones Científicas y Técnicas (CONICET), Argentina.*
[7] *Instituto de Astrofísica e Ciências do Espaço, Universidade do Porto, CAUP, Rua das Estrelas, 4150-762 Porto, Portugal.*
[8] *Instituto de Astronomía, Universidad Nacional Autónoma de México, Cd. Universitaria, México, D.F. 04510, México.*

Accepted 2018. Received 2018; in original form 2018

ABSTRACT

Motivated by the challenges of calculating the dynamical masses of late-type galaxies (LTGs) and the enormous amount of data from the Sloan Digital Sky Survey (SDSS), we calculate virial masses of a sample of approximately 126,000 LTGs from the sixteenth data release of the SDSS. The virial mass estimations were made considering Newtonian mechanics, virial equilibrium and velocity dispersion from stars and gas. The procedure gave as a result seven mass estimations for each galaxy. The calculated masses were calibrated using a sample of spiral galaxies with velocity rotation curves. Considering the results from the calibration, we find that the correlation between virial and dynamical (rotation curve) masses is stronger for high inclination values. Therefore the calibration relies more on the available data for higher inclination angle galaxies. We also show that if we have a heterogeneous sample of galaxies one must take into consideration the size and colour of these galaxies by using the following variables: Sersic index n, concentration index and colour of the stars. For relatively smaller and bluer LTGs the gas velocity dispersion provides a more consistent mass calculation, while for LTGs that are relatively larger and redder the stellar velocity dispersion provides a better correlated mass calculation.

Key words: Galaxies: fundamental parameters. Galaxies: photometry, distances and redshifts.

1 INTRODUCTION

The determination of the masses of galaxies has been an interesting problem ever since galaxies were identified as very large conglomerations of stars and gas in the universe (see Burbidge & Burbidge 1975; Fich & Tremaine 1991; Courteau et al. 2014). At present there are three main methods that allow the calculation of galactic masses, namely:

(i) Dynamical or virial masses. The dynamical or virial masses are determined recurring to dynamical methods which in turn use the rotation curves or the velocity dispersion of gas or stars in galaxies. It is important to mention at this point that all these methods presuppose that Newtonian gravitation is valid at all scales in the universe; if this were not the case, then the determinations obtained from these methods would be flawed. The dynamical mass

⋆ E-mail: alberto.nigoche@academicos.udg.mx eduardo.delafuente@academicos.udg.mx

determinations for LTGs are usually derived from their rotation curves. Early attempts to determine the masses of galaxies using this method were undertaken by Scheiner (1899), Slipher (1914), Pease (1918), and Opik (1922), in which he inferred a value for the mass of M31. Some time later there were attempts at determining the mass of the Milky Way by Kapteyn & van Rhijn (1922), Oort (1932b), and Oort (1932a). Determinations of the M31 total mass using velocities determined from absorption lines were made by Babcock (1939), Mayall (1950), and Lallemand et al. (1960). With the measurement of rotation curves further away from the centre of LTGs, and the discovery that these remain flat out to large radii, early suggestions of the existence of a non-luminous massive component were put forward. Rubin & Ford (1970) were the first to obtain a rotation curve for M31 out to 120′ ($\sim 27\ kpc$) in which they noticed how it remains flat out to a large distance from the centre. Using HI, Roberts & Whitehurst (1975) confirmed the flatness of the M31 rotation curve out to 170′ ($\sim 38\ kpc$). The flatness of rotation curves in all galaxy types is a well-established fact (Faber & Gallagher 1979; Rubin et al. 1985; Sofue & Rubin 2001, among others). There have also been mass determination of LTGs using the emission lines of $H\alpha$, CO and HI. A reasonable agreement between determinations performed with these different lines is found (see Sofue & Rubin 2001; Simon et al. 2003, 2005; Spekkens & Sellwood 2007)), and also from measurements made with the $[OII]$, $[OIII]$, $H\beta$ and $[SII]$ lines (Courteau & Sohn 2003). At some point the question of whether the gas rotation curve really represented the total mass of the galaxy arose. There is likely evidence that the gas rotation curves represent the gas distribution within the optical disk of galaxies (see Cayatte et al. 1994; Mathewson et al. 1992; Courteau 1997; Catinella et al. 2007, among others).

To determine the mass of an elliptical galaxy using the virial theorem, three things are needed:

- Distance of the galaxy from the Sun
- the line-of-sight velocity dispersion of the stars in the centre
- the distribution of light projected on the plane of the sky from which we can derive the potential energy

The first determination of a velocity dispersion was for $M32$ by Minkowsky (1954), later Burbidge et al. (1961c) and Burbidge et al. (1961b) reevaluated the value of the velocity dispersion and in Burbidge et al. (1961a) they obtained the velocity dispersion for NGC 3379. Velocity dispersions for 12 additional galaxies were obtained by Minkowsky (1961). For the determination of the potential energy of a spheroidal galaxy we refer to Poveda (1958) where a full discussion is given. It was shown by de Vaucouleurs (1963) and Poveda (1958) that the potential energy is given by:

$$\Omega = -0.33\frac{GM^2}{R'} \quad (1)$$

where R' is the radius that contains half of the total light of the galaxy, this radius is called the 'effective' radius, G is the constant of Universal Gravitation and M represents the mass. All the quantities in equation (1) are in cgs units.

The dynamical masses of Gas-Poor Galaxies ($ETGs$) have been determined from molecular gas observations by Sage et al. (2007) and Young et al. (2011), from ionised gas observations by Bertola et al. (1984), Fisher (1997) and Sarzi et al. (2006) and from neutral gas observations by Knapp et al. (1985), Morganti et al. (2006), and di Serego Alighieri et al. (2007) among others. King & Minkowski (1966) measured rotation in the inner regions of two giant ellipticals in the Virgo cluster, NGC 4621 (E3) and NGC 4697 (E5).

(ii) Luminous masses. Luminous masses of galaxies are determined measuring the total luminosity of galaxies and assuming a specific mass to light (M/L) ratio which would imply a value for the mass. The (M/L) does not have a universal value and its determination is central to the calculation of galaxy masses using this method. The (M/L) ratio may depend on a variety of factors such as the way the galactic mass is assembled (De Lucia et al. 2007), the different Spectral Energy Distributions (SED) of galaxies (Walcher et al. 2011) and (Conroy 2013), the different mix of Stellar Populations (SPs). Oort (1926) and Baade (1944) recognized the presence of at least two different SPs in our galaxy. For a comprehensive review on SPs see Greggio & Renzini (2011). The different SPs are superposed in a galaxy, and each has a different Star Formation Rate (SFR) which must also be considered and which evolves with time (Sandage 1986), (MacArthur et al. 2004). Another factor is the Initial Mass Function (IMF; see Salpeter 1955; Scalo 1986; Kroupa 2001; Chabrier 2003) which tells us how the mass is distributed in a galaxy at the beginning of the lives of its stars.

The types of stars in a galaxy -hence their mass- can be calculated using stellar population synthesis models. There are optimised population synthesis models (see Spinrad & Taylor 1971; Faber 1972; O'Connell 1976; Pickles 1985; Bica & Alloin 1986; MacArthur et al. 2009, among others) and Evolutionary population synthesis models (see Tinsley 1972; Tinsley & Gunn 1976; Renzini & Voli 1981; Bruzual A. 1983, among others). In summary, determining the M/L ratio for a galaxy could be a very complicated problem, however once it is determined, the galactic mass can be calculated straightforwardly from its measured luminosity and distance.

(iii) Mass determination using relativistic light bending by gravitational lenses. This method would give us a crude value for the mass of a single galaxy because in order to bend light gravitationally it is necessary to have a very large mass such as that of a cluster of galaxies and the mass of an individual galaxy would correspond to the average value of the mass for each galaxy in the cluster.

The first attempt to detect the weak gravitational bending of light by a massive object was conducted by Tyson et al. (1984) with a not very definitive result, the first real detection was achieved by Brainerd et al. (1996). Mass measurements for galaxies in the Sloan Digital Sky Survey (SDSS) were achieved by McKay et al. (2002) and Prada et al. (2003). Dark matter was detected by Kaiser & Squires (1993) and lensing produced by clusters of galaxies was detected by Tyson et al. (1990), and Fahlman et al. (1994). There have been a number of searches for spiral lens galaxies by Féron et al. (2009), Sygnet et al. (2010) and Treu et al. (2011).

The Hubble Space Telescope (*HST*) has been used to take data on weak lensing galaxies for a few tens of ETGs with $0.1 \leqslant z \leqslant 0.8$ see (Gavazzi et al. 2007), (Auger et al. 2010), (Lagattuta et al. 2010).

There is also what is called Strong Gravitational Lensing. There is a multitude of papers that have either tried to detect it or have detected it and in so doing, one of their byproducts has been the measurement of masses of clusters of galaxies. Papers such as those by Bertin et al. (1992), Saglia et al. (1992), Loewenstein & White (1999), Keeton (2001), and Padmanabhan et al. (2004) to mention a few.

There have been a few strong lensing surveys such as SLACS (Sloan Lens ACS) Bolton et al. (2004), Bolton et al. (2005), Bolton et al. (2006), Bolton et al. (2008),Schneider (2006), Koopmans et al. (2006), Treu et al. (2006), Treu et al. (2009), Gavazzi et al. (2007),Treu (2010), Auger et al. (2011) and Newton et al. (2011) among others.

In order to apply the first two methods (dynamics, luminosity) it is necessary to know the distance at which the galaxy in question is located. The further away this galaxy is, the larger the uncertainties in the distance determination, and therefore the larger the uncertainties in its mass.

In the case of LTGs, they contain different structures (bulge, disk, spiral arms) with different levels of importance that make it difficult to calculate the dynamical or the virial mass properly because the tracers of these structures are different. The best way to obtain the dynamical mass of LTGs is using the rotation curves but the present-day technology is not good enough to obtain these rotation curves for relatively distant LTGs. Besides the amount of time to obtain the rotation curves of LTGs is relatively high. At the present time, we can find in the literature photometric and spectroscopic information of thousands of galaxies from different surveys, but this information is not sufficient to obtain the rotation curves due to the previously mentioned problems. However, the SDSS contains more than one hundred thousand LTGs with photometric and spectroscopic information that can be used to obtain their virial masses through the velocity dispersion of gas and/or stars. This work is devoted to using this valuable information from the SDSS and obtaining virial mass estimations of LTGs with the lowest possible uncertainties. To achieve this goal we will use a subsample of SDSS LTGs with measured rotation curves from the literature to obtain their dynamical mass and compare it with the virial mass estimation from the velocity dispersion. This comparison will permit us to calibrate the virial masses, taking into account the importance of the different structures that constitute the LTGs.

This work is organized as follows: In section 2 we present our sample of galaxies and the method by which it was selected. Section 3 presents the formal definition of dynamic and virial masses. In section 4 we calculate the virial masses of the galaxies in our sample. In section 5 we calculate the dynamical masses of a subsample of galaxies which have rotation curves determined in the literature. Section 7 presents the comparison of the virial and dynamical masses. In section 8 we discuss our findings and finally in section 9 we present our conclusions.

2 THE SAMPLE OF LTGS

We extract a sample of LTGs -exponential brightness profile- from the SDSS DR16 (York et al. 2000; Blanton et al. 2003) with photometric and spectroscopic information. The basic required parameters to achieve the goals of this work are size and velocity dispersion from stars and gas. The main selection criterion used to quantify the brightness profile was the SDSS $fracDeV$ parameter. The $fracDeV$ parameter is equivalent to the Sersic (1968) index n, $n = 1$ corresponds to $fracDeV = 0$ while $n = 4$ corresponds to $fracDeV = 1$. Galaxies with $fracDeV < 0.5$ are relatively well adjusted by a exponential profile. Since the photometric errors are lower in g and r filters and the spectroscopic errors are lower for velocity dispersion greater than 60 km/s, we take into account this information to obtain the sample of LTGs. The resultant sample with $fracDeV_g < 0.5$, $fracDeV_r < 0.5$ and stellar $\sigma > 60$ km/s -according to SDSS nomenclature- contains 126 815 galaxies. These galaxies are distributed in a redshift interval $0.00 < z < 0.35$ and within a magnitude range $\Delta m \sim 10$ mag.

2.1 Correction of the photometric and spectroscopic data

Once we have compiled the galaxy sample, we must correct both the photometric and the spectroscopic data. We here list the performed corrections (see Nigoche-Netro et al. 2015):

- Seeing and Extinction corrections: we use the seeing-corrected parameters in the total magnitude and effective radius as well as the extinction corrections by employing the respective SDSS pipelines on the data (see York et al. 2000; Blanton et al. 2003, and references therein).
- K correction: We use the values obtained from the following formulae (Nigoche-Netro et al. 2008):

$$k_g(z) = -5.261 z^{1.197}, \quad (2)$$

$$k_r(z) = -1.271 z^{1.023}, \quad (3)$$

• Cosmological dimming correction: We follow Jørgensen et al. (1995a) where the effective surface brightness ($<\mu_e>$) is corrected by subtraction of 10 log(1+z), being z the redshift relative to the CMB.

• Evolution correction: We apply the evolution correction from Nigoche-Netro et al. (2008) utilising:

$$ev_g(z) = +1.15z, \tag{4}$$

$$ev_r(z) = +0.85z, \tag{5}$$

• Effective radius correction to the rest reference frame: We follow Hyde & Bernardi (2009) to correct colour gradients where the mean effective radius is smaller at longer wavelengths by using:

$$r_{e,g,rest} = \left[\frac{(1+z)\lambda_g - \lambda_r}{\lambda_g - \lambda_r}\right](r_{e,g,obs} - r_{e,r,obs}) + r_{e,r,obs}, \tag{6}$$

with $\lambda_g = 4686$Å, and $\lambda_r = 6165$Å.

• Aperture correction to the velocity dispersion: The aperture correction is significant because it avoids dependencies on distance and instruments used in calculating the spectral parameters. Following Jørgensen et al. (1995b), we determine the ratio between the velocity dispersion values (σ_{SDSS}) and the corrected velocity dispersion (σ_e) or velocity dispersion inside r$_e$ as:

$$log\left(\frac{\sigma_{SDSS}}{\sigma_e}\right) = -0.065log\left(\frac{r_{ap}}{r_e}\right) - 0.013\left[log\left(\frac{r_{ap}}{r_e}\right)\right]^2, \tag{7}$$

where $r_{ap} = 1.5$ arcsec for the SDSS case (York et al. 2000; Blanton et al. 2003).

Finally, the errors in the photometric and spectroscopic variables were obtained from the errors given in the SDSS, which were in turn propagated by considering the mathematical expressions of each of the corrections listed above.

3 THE MASS ESTIMATIONS OF THE LTGS

We assume Newtonian dynamics and that the velocity dispersion is due to the gravitational potential well. The LTGs mass estimates are made using data for stars and gas obtained from the SDSS DR16. These estimates will be calibrated later by means of a sample of galaxies for which we have measured rotation curves.

We have defined the virial masses as those masses that are obtained using the velocity dispersion of the gas or of the stars in the galaxies, while the dynamical masses would be those masses obtained by means of the rotation curves. It is important to stress that this nomenclature is used as a means to differentiate the method by which the masses are obtained, however both mass-values are due to the gravitational potential of the galaxy in question and are derived using Newtonian dynamics.

4 THE VIRIAL MASS FROM THE STARS OF LTGS.

We have made seven estimates of the total virial mass ($\mathbf{M_{Virial}}$) (see section 4.1) considering the following equation (Poveda 1958):

$$\mathbf{M_{Virial}} \sim K\frac{r_e\sigma_e^2}{G}, \tag{8}$$

where r_e and, σ_e represent the effective radius and the velocity dispersion of stars inside r_e, respectively, G is the gravitational constant and K is the proportion or scale factor. Historically, the scale factor has been considered constant, for example, for the de Vaucouleurs profile case Cappellari et al. (2006) found $K = 5.9$. Further studies have found the scale factor seems to depend on the Sersic index and/or the inclination angle of the galactic plane (Cappellari et al. 2006; Mocz et al. 2012). In this work we will consider both constant and variable scale factor (see section 4.1). This scale factor will be calibrated with the analysis that we will perform in the following sections.

Equation 8 considers an idealized situation and does not take into account possible effects on the mass estimations of LTGs due to environment, shape and velocity dispersion anisotropies.

4.1 Calculation of virial masses considering different scale factors and different estimates of the velocity dispersion

As previously mentioned the data for the virial mass estimates for the LTGs have been taken from the SDSS DR16. The data used are: the redshift, the exponential effective radius, the Petrosian radii R90 and R50, the major and minor semi-axes of the galactic disk, the stellar velocity dispersion, the gas velocity dispersion using the H_α line, and the gas velocity dispersion using the average of some of the Balmer lines ($H_\alpha, H_\gamma, H_\beta, H_\delta, H_\epsilon, H_\zeta, H_\eta$). In what follows we present these estimates.

(i) $\mathbf{M_{KS}}$. This mass was calculated using a constant scale factor (K=5.9) and the velocity dispersion of the stars.

(ii) $\mathbf{M_{KA}}$. This mass was calculated using a constant scale factor (K=5.9) and the velocity dispersion of H_α.

(iii) $\mathbf{M_{KB}}$. This mass was calculated using a constant scale factor (K=5.9) and the average of the velocity dispersion of the Balmer lines.

(iv) $\mathbf{M_{nS}}$. This mass was calculated using a scale factor as a function of the Sersic index n ($K = 8.87 - 0.831n + 0.0241n^2$) (Cappellari et al. 2006) and the velocity dispersion of the stars.

For the remaining three estimates we considered K as a function of the galactic inclination angle (i) (Mocz et al. 2012) as expressed in the following equations:

$$K = \left(\frac{2.3548}{sin(i)}\right)^2, \tag{9}$$

$$sin(i) = \sqrt{\frac{1-(\frac{b}{a})^2}{1-(0.19)^2}}, \tag{10}$$

where a and b represent the major and minor semi-axes of the galactic disk.

(v) $\mathbf{M_{IS}}$. This mass was calculated using a scale factor expressed as a function of the inclination angle (equation 9) and the velocity dispersion of the stars.

(vi) $\mathbf{M_{IA}}$. This mass was calculated using a scale factor expressed as a function of the inclination angle (equation 9) and the velocity dispersion of H_α.

(vii) $\mathbf{M_{IB}}$. This mass was calculated using a scale factor expressed as a function of the inclination angle (equation 9) and the average of the velocity dispersion of the Balmer lines.

In table A.1 (appendix A) we show an extract (145 LTGs) of the virial masses catalogue, of the 126 815 LTGs, obtained following the previous procedures. The entire catalogue could be found, in electronic form, in the following link:

5 DYNAMICAL MASSES OF A SUBSAMPLE OF LTGS USING ROTATION CURVES

Catinella et al. (2005) presented a long slit spectroscopic study in H_α of 403 non-interacting spiral galaxies using the Palomar Hale 5 m telescope. One of the main objectives of this study was to obtain their rotation curves. In this work we selected all the galaxies from Catinella et al. (2005) which have photometric and spectroscopic information in the SDSS DR16 sample, resulting in a subsample of 145 galaxies. The spectroscopic information includes the stellar velocity dispersion and/or the gas velocity dispersion.

In what follows we present the details of the calculation of the dynamical mass for the 145 Catinella et al. (2005) galaxies using their rotation curves. We make available the results in Table A2.

In order to determine the dynamical masses of the LTGs, a mass component fitting was performed. The mass components were represented by a Miyamoto-Nagai Potential (Miyamoto & Nagai 1975):

$$\phi = \frac{GM}{\sqrt{R^2 + \left[a + (b^2+z^2)^{1/2}\right]^2}}, \tag{11}$$

where G is the universal gravitational constant and M the total mass generating the gravitational field; a and b are two constants representing the scale length and scale height respectively, whereas R and z are the spatial variables.

A disk was set as the main component. Depending on the quality of the kinematic data, a second spherical inner component was included. Additionally, for some objects, an external spherical component was required to account for the flat region of the rotation curves at large radii. The obtained masses were corrected by inclination following the SDSS DR16 data. Respect to the fitting process, the main difficulties came from the deviation from circular motion which is present in almost all LTGs. Other aspects such as the spatial sampling, the radial extension of kinematic data and the rotational center determination were also considered as source of uncertainties. The obtained dynamical masses and their errors are listed in Appendix A (Table A.2).

If we only consider the information on galaxies with relatively small errors (less than 30% in both virial and dynamical mass) and difference between virial and dynamical masses less than three times the dispersion (see Tables 1-6), the sample is reduced to a total of approximately 80 galaxies, with small variations in the total number depending on the subsample selection criteria. We used these subsamples in the following sections to perform the calibration of the virial masses.

6 SUBSAMPLES DEFINITION FOR THE COMPARISON OF VIRIAL AND DYNAMICAL MASSES

The estimates of the virial and/or dynamical masses may be dependent on different properties, including the following: absolute magnitude, Sersic index, concentration index, colour ($g-r$) and galactic inclination angle. So, in order to perform the comparison in an appropriate manner we must consider subsamples with different cuts in the variables mentioned above. The estimation of the variable is described as follows:

- The absolute magnitude was calculated considering the corrected apparent magnitude and the redshift from the SDSS.
- The Sersic index was calculated through a fit to the n vs. R90/R50 from Table 1 in Graham et al. (2005) in filters g and r from the SDSS, and later we took the average of these indices. R90 and R50 are the radii that contain 90% and 50% of the Petrosian flux, respectively.
- The concentration parameter was obtained by averaging the ratio of the Petrosian radii (R90/R50) from the SDSS in the filters g and r.
- The colour $g-r$ was obtained from the g and r corrected magnitudes in the SDSS.
- The average inclination angle was calculated from equation 3 in filters g and r from SDSS.

Table 1. $BCES_{Bis}$ fit parameters for $\mathbf{M_{Virial}}$ vs. $\mathbf{M_{Dyn}}$ for LTG samples considering different scale factors and distinct estimates of the velocity dispersion (see Section 4.1). We apply approximately symmetric cuts in the values of absolute magnitude in the g filter M_g.

	Slope	Intercept	Correlation coefficient	Dispersion	No. of galaxies
M_g > -20.2					
$\mathbf{M_{KS}}$	1.11 ± 0.09	-0.61 ± 0.90	0.77	0.29	31
$\mathbf{M_{KA}}$	1.11 ± 0.10	-0.51 ± 1.02	0.71	0.27	23
$\mathbf{M_{KB}}$	1.15 ± 0.19	-0.92 ± 1.89	0.42	0.30	31
$\mathbf{M_{nS}}$	1.09 ± 0.08	-0.49 ± 0.80	0.78	0.28	39
$\mathbf{M_{IS}}$	1.08 ± 0.09	-0.34 ± 1.00	0.71	0.33	40
$\mathbf{M_{IA}}$	0.94 ± 0.08	1.18 ± 0.81	0.72	0.27	33
$\mathbf{M_{IB}}$	1.08 ± 0.21	-0.18 ± 2.06	0.32	0.33	31
M_g ⩽ -20.2					
$\mathbf{M_{KS}}$	1.16 ± 0.06	-1.39 ± 0.68	0.74	0.28	52
$\mathbf{M_{KA}}$	0.94 ± 0.06	1.10 ± 0.60	0.68	0.29	47
$\mathbf{M_{KB}}$	0.93 ± 0.05	1.29 ± 0.56	0.72	0.28	46
$\mathbf{M_{nS}}$	1.17 ± 0.07	-1.62 ± 0.73	0.72	0.29	54
$\mathbf{M_{IS}}$	1.06 ± 0.07	-0.28 ± 0.75	0.74	0.25	53
$\mathbf{M_{IA}}$	0.94 ± 0.08	1.02 ± 0.90	0.58	0.34	50
$\mathbf{M_{IB}}$	0.95 ± 0.08	1.10 ± 0.88	0.62	0.34	50

Table 2. $BCES_{Bis}$ fit parameters for $\mathbf{M_{Virial}}$ vs. $\mathbf{M_{Dyn}}$ for LTG samples considering different scale factors and distinct estimates of the velocity dispersion (see Section 4.1). We apply approximately symmetric cuts in the values of Sersic index n.

	Slope	Intercept	Correlation coefficient	Dispersion	No. of galaxies
$n \leqslant 0.8$					
$\mathbf{M_{KS}}$	0.87 ± 0.05	1.92 ± 0.52	0.82	0.22	40
$\mathbf{M_{KA}}$	0.85 ± 0.04	2.17 ± 0.39	0.86	0.24	37
$\mathbf{M_{KB}}$	0.94 ± 0.03	1.13 ± 0.31	0.89	0.22	36
$\mathbf{M_{nS}}$	0.89 ± 0.04	1.48 ± 0.49	0.84	0.25	46
$\mathbf{M_{IS}}$	0.87 ± 0.05	1.77 ± 0.49	0.82	0.26	47
$\mathbf{M_{IA}}$	0.83 ± 0.04	2.28 ± 0.44	0.85	0.26	42
$\mathbf{M_{IB}}$	0.93 ± 0.03	1.22 ± 0.33	0.85	0.25	39
$n > 0.8$					
$\mathbf{M_{KS}}$	1.12 ± 0.04	-0.88 ± 0.42	0.86	0.30	43
$\mathbf{M_{KA}}$	0.99 ± 0.05	0.59 ± 0.55	0.79	0.32	34
$\mathbf{M_{KB}}$	1.02 ± 0.04	0.41 ± 0.46	0.82	0.30	41
$\mathbf{M_{nS}}$	1.08 ± 0.04	-0.47 ± 0.39	0.85	0.31	47
$\mathbf{M_{IS}}$	1.01 ± 0.03	0.38 ± 0.33	0.87	0.29	46
$\mathbf{M_{IA}}$	0.94 ± 0.07	1.14 ± 0.69	0.82	0.34	41
$\mathbf{M_{IB}}$	0.99 ± 0.08	0.70 ± 0.80	0.78	0.36	42

Table 3. $BCES_{Bis}$ fit parameters for $\mathbf{M_{Virial}}$ vs. $\mathbf{M_{Dyn}}$ for LTG samples considering different scale factors and distinct estimates of the velocity dispersion (see Section 4.1). We apply approximately symmetric cuts in the concentration parameter (R90/R50).

	Slope	Intercept	Correlation coefficient	Dispersion	No. of galaxies
(R90/R50) ⩽ 2.4					
$\mathbf{M_{KS}}$	0.93 ± 0.04	1.23 ± 0.47	0.84	0.21	37
$\mathbf{M_{KA}}$	0.82 ± 0.04	2.43 ± 0.38	0.88	0.21	35
$\mathbf{M_{KB}}$	0.92 ± 0.03	1.38 ± 0.29	0.90	0.20	33
$\mathbf{M_{nS}}$	0.97 ± 0.04	0.66 ± 0.48	0.85	0.24	42
$\mathbf{M_{IS}}$	0.94 ± 0.04	0.97 ± 0.48	0.85	0.25	41
$\mathbf{M_{IA}}$	0.84 ± 0.04	2.14 ± 0.38	0.88	0.25	38
$\mathbf{M_{IB}}$	0.89 ± 0.03	1.51 ± 0.34	0.86	0.23	35
(R90/R50) >2.4					
$\mathbf{M_{KS}}$	1.06 ± 0.03	-0.22 ± 0.32	0.86	0.30	46
$\mathbf{M_{KA}}$	0.93 ± 0.04	1.31 ± 0.45	0.81	0.30	35
$\mathbf{M_{KB}}$	0.95 ± 0.04	1.09 ± 0.39	0.82	0.31	44
$\mathbf{M_{nS}}$	1.04 ± 0.03	-0.12 ± 0.35	0.86	0.30	51
$\mathbf{M_{IS}}$	0.95 ± 0.03	0.96 ± 0.31	0.86	0.29	52
$\mathbf{M_{IA}}$	0.89 ± 0.06	1.67 ± 0.62	0.83	0.33	45
$\mathbf{M_{IB}}$	0.94 ± 0.07	1.27 ± 0.69	0.77	0.36	46

Table 4. $BCES_{Bis}$ fit parameters for $\mathbf{M_{Virial}}$ vs. $\mathbf{M_{Dyn}}$ for LTG samples considering different scale factors and distinct estimates of the velocity dispersion (see Section 4.1). We apply approximately symmetric cuts in the values of color $g - r$.

	Slope	Intercept	Correlation coefficient	Dispersion	No. of galaxies
$g - r \leqslant 0.6$					
$\mathbf{M_{KS}}$	0.82 ± 0.05	2.41 ± 0.57	0.85	0.24	30
$\mathbf{M_{KA}}$	0.81 ± 0.03	2.54 ± 0.35	0.89	0.20	32
$\mathbf{M_{KB}}$	0.93 ± 0.04	1.39 ± 0.37	0.85	0.24	38
$\mathbf{M_{nS}}$	0.85 ± 0.04	1.98 ± 0.49	0.83	0.27	41
$\mathbf{M_{IS}}$	0.82 ± 0.05	2.37 ± 0.53	0.82	0.28	40
$\mathbf{M_{IA}}$	0.81 ± 0.03	2.48 ± 0.34	0.89	0.24	39
$\mathbf{M_{IB}}$	0.86 ± 0.04	2.03 ± 0.44	0.83	0.26	40
$g - r > 0.6$					
$\mathbf{M_{KS}}$	1.19 ± 0.04	-1.64 ± 0.45	0.83	0.29	54
$\mathbf{M_{KA}}$	0.99 ± 0.05	0.56 ± 0.58	0.76	0.33	38
$\mathbf{M_{KB}}$	1.07 ± 0.05	-0.11 ± 0.54	0.76	0.35	39
$\mathbf{M_{nS}}$	1.21 ± 0.04	-2.02 ± 0.46	0.83	0.29	52
$\mathbf{M_{IS}}$	1.11 ± 0.04	-0.79 ± 0.42	0.84	0.27	53
$\mathbf{M_{IA}}$	0.93 ± 0.08	1.24 ± 0.81	0.72	0.36	44
$\mathbf{M_{IB}}$	1.01 ± 0.08	0.44 ± 0.79	0.71	0.38	41

Table 5. $BCES_{Bis}$ fit parameters for $\mathbf{M_{Virial}}$ vs. $\mathbf{M_{Dyn}}$ for LTG samples considering different scale factors and distinct estimates of the velocity dispersion (see Section 4.1). We apply color cuts considering the lower limit of the red sequence ($\psi = -0.02667M_r + 0.11333$) (Cooper et al. 2010).

	Slope	Intercept	Correlation coefficient	Dispersion	No. of galaxies
$g - r \leqslant \psi$					
$\mathbf{M_{KS}}$	0.88 ± 0.05	1.73 ± 0.58	0.81	0.27	48
$\mathbf{M_{KA}}$	0.87 ± 0.04	1.91 ± 0.43	0.82	0.27	47
$\mathbf{M_{KB}}$	0.94 ± 0.04	1.25 ± 0.39	0.82	0.27	55
$\mathbf{M_{nS}}$	0.87 ± 0.05	1.73 ± 0.49	0.82	0.28	59
$\mathbf{M_{IS}}$	0.83 ± 0.07	2.22 ± 0.78	0.76	0.32	60
$\mathbf{M_{IA}}$	0.84 ± 0.05	2.18 ± 0.56	0.82	0.32	53
$\mathbf{M_{IB}}$	0.87 ± 0.04	1.97 ± 0.38	0.81	0.27	56
$g - r > \psi$					
$\mathbf{M_{KS}}$	1.21 ± 0.03	-1.77 ± 0.43	0.88	0.26	35
$\mathbf{M_{KA}}$	0.96 ± 0.03	0.97 ± 0.53	0.84	0.27	23
$\mathbf{M_{KB}}$	1.02 ± 0.04	0.39 ± 0.42	0.83	0.32	24
$\mathbf{M_{nS}}$	1.25 ± 0.03	-2.28 ± 0.47	0.89	0.25	34
$\mathbf{M_{IS}}$	1.17 ± 0.03	-1.42 ± 0.41	0.89	0.26	33
$\mathbf{M_{IA}}$	0.93 ± 0.03	1.24 ± 0.36	0.86	0.26	30
$\mathbf{M_{IB}}$	1.02 ± 0.05	0.41 ± 0.51	0.82	0.34	25

Table 6. $BCES_{Bis}$ fit parameters for $\mathbf{M_{Virial}}$ vs. $\mathbf{M_{Dyn}}$ for LTG samples considering different scale factors and distinct estimates of the velocity dispersion (see Section 4.1). We apply approximately symmetric cuts in the values of inclination angle i.

	Slope	Intercept	Correlation coefficient	Dispersion	No. of galaxies
$i \leqslant 66$					
$\mathbf{M_{KS}}$	1.19 ± 0.06	-1.66 ± 0.65	0.79	0.32	43
$\mathbf{M_{KA}}$	0.97 ± 0.04	0.79 ± 0.47	0.81	0.29	34
$\mathbf{M_{KB}}$	1.10 ± 0.05	-0.58 ± 0.49	0.83	0.30	34
$\mathbf{M_{nS}}$	1.15 ± 0.04	-1.36 ± 0.48	0.84	0.30	46
$\mathbf{M_{IS}}$	1.07 ± 0.05	-0.47 ± 0.54	0.84	0.29	46
$\mathbf{M_{IA}}$	0.94 ± 0.06	0.99 ± 0.66	0.81	0.33	42
$\mathbf{M_{IB}}$	1.12 ± 0.08	-0.91 ± 0.83	0.76	0.36	38
$i > 66$					
$\mathbf{M_{KS}}$	0.92 ± 0.02	1.37 ± 0.24	0.90	0.23	40
$\mathbf{M_{KA}}$	0.86 ± 0.04	2.08 ± 0.38	0.86	0.25	36
$\mathbf{M_{KB}}$	0.85 ± 0.03	2.16 ± 0.32	0.86	0.24	43
$\mathbf{M_{nS}}$	0.92 ± 0.02	1.25 ± 0.26	0.89	0.24	47
$\mathbf{M_{IS}}$	0.89 ± 0.02	1.68 ± 0.26	0.89	0.24	47
$\mathbf{M_{IA}}$	0.86 ± 0.02	2.00 ± 0.24	0.89	0.24	41
$\mathbf{M_{IB}}$	0.85 ± 0.03	2.17 ± 0.32	0.87	0.24	43

7 CALIBRATION OF THE DYNAMICAL MASSES OF THE SDSS LTGS SAMPLE

In order to make the comparison between the dynamical and virial masses, we divide the samples in an approximately symmetrical way with respect to the different variables that might affect the estimates of the virial mass (see section 6). In Figure 1 we show a mosaic of the frequency distribution of the mentioned variables with the objective that the reader can visualize where the cuts were performed, dividing the sample approximately equally. Due to the different ways of calculating the masses and the number of variables investigated there are potentially more than 40 graphs that could be presented, but here we only show the graphs of one of the biggest samples ($\mathbf{M_{nS}}$ sample) to avoid giving redundant information.

Once the cuts are made we perform a linear fit to the data. The coefficients of the fit could be affected significantly by both the choice of independent variables and the fitting method (Isobe et al. 1990). The measurement errors in the variables may induce even bigger biases, as well as correlation in the errors or intrinsic dispersion in the relation. The Bivariate Correlated Errors and Intrinsic Scatter Bisector ($BCES_{Bis}$) method (Isobe et al. 1990; Akritas & Bershady 1996; Nigoche-Netro et al. 2010) is a statistical model that takes into account the different sources of bias mentioned above. Here, we use the $BCES_{Bis}$ method to calculate the coefficients of the $\mathbf{M_{Virial}}$ vs. $\mathbf{M_{Dyn}}$ relationships. The results are as follows:

(i) Absolute magnitude cut in the filter g (M_g).

The absolute magnitude cut was made at M_g = -20.2. In Table 1 and Figure 2 we show the comparison between the virial and dynamical masses for the seven estimates of the virial mass with $M_g >$ -20.2 and $M_g \leqslant$ -20.2.

(ii) Sersic index cut.

The cut in the Sersic index n was taken at n = 0.8. In Table 2 and Figure 3 we show the results for the comparison of the virial and dynamical masses for the seven estimates of the virial mass with $n >$ 0.8 and $n \leqslant$ 0.8.

(iii) Concentration cut (R90/R50).

The cut in concentration was made at (R90/R50) = 2.4. In Table 3 and Figure 4 we show the results of comparing the virial and dynamical masses for the seven estimates of the virial mass with (R90/R50) > 2.4 and (R90/R50) $\leqslant$ 2.4.

(iv) Colour g-r cut.

The colour cut was taken in two different ways:

- Symmetrical cut in g-r = 0.6. In Table 4 and Figure 5 we show the results for the comparison of virial and dynamical masses for the seven estimates of the virial mass with g-r > 0.6 and g-r $\leqslant$ 0.6.

- Knowing that the galaxies, including the spiral galaxies, are found in two well differentiated regions on a colour-magnitude diagram (the red sequence on the top part and the blue cloud on the bottom part; see Figure 6) we performed a cut in the colour g-r considering the following lower limit to the red sequence (ψ) (Cooper et al. 2010):

$\psi = -0.02667 M_r + 0.11333$

In Table 5 and in Figure 7 we show the results of the comparison of the virial and dynamical masses for the seven estimates of the virial mass with $g - r > \psi$ and $g - r \leqslant \psi$.

(v) Cut in inclination angle (i).

The cut in inclination angle was made at $i = 66^{\circ}$. In Table 6 and Figure 8 we show the results of the comparison for the virial and dynamical masses for the seven estimates of the virial mass with $i > 66^{\circ}$ and $i \leqslant 66^{\circ}$.

8 DISCUSSION

The comparisons of the virial and dynamical masses from the different samples of LTGs gave the following results:

- When the magnitude is considered in the comparison of subsamples of LTGs we find that the correlation coefficients attain the lowest values and the fit dispersions attain the highest values with respect to the rest of the variables considered in the analysis (Sersic index n, concentration, colour, and angle of inclination).

There are neither substantial differences in the correlation fits nor in the dispersion when we compare samples of faint and bright galaxies (see Figure 2 and Table 1). The method used to make the estimate of the virial mass is of no consequence, that is to say, there are no significant differences whether the virial mass is obtained with a constant K or if it is dependent on the Sersic n index or the inclination angle. It also does not matter whether this virial mass was obtained using the velocity dispersions of the stars or of the gas.

- When we consider the Sersic index n, the correlation is relatively high in all fits (see Table 2). We can see that for $n \leqslant 0.8$ the slopes are lower than the slopes for $n > 0.8$. It is noticeable that for galaxies with $n \leqslant 0.8$ the correlation is lower when the virial mass is obtained using the stars compared to when this mass is obtained using the gas. For galaxies with $n > 0.8$ the opposite occurs. The method by which the virial mass is obtained turns out not to be significant for these results.

- When we consider the LTGs concentration parameter (R90/R50), we can see that for R90/R50 < 2.4 the slopes are lower than the slopes for R90/R50 > 2.4 (see Table 3). We also find a relatively high correlation for all fits. In this case, we observe that the more concentrated LTGs (R90/R50 < 2.4) show a larger correlation, when we use the gas in estimating the virial mass, as opposed to when we use the stars. For the less concentrated galaxies (R90/R50 > 2.4) the opposite occurs. The method by which the virial mass is calculated does not seem to be of much importance for these results.

- When the LTGs color is considered, we can see that for blue galaxies the slopes are lower than the slopes for red galaxies (see Tables 4 and 5). We also find a relatively high correlation in all cases. It can be noticed that for blue galax-

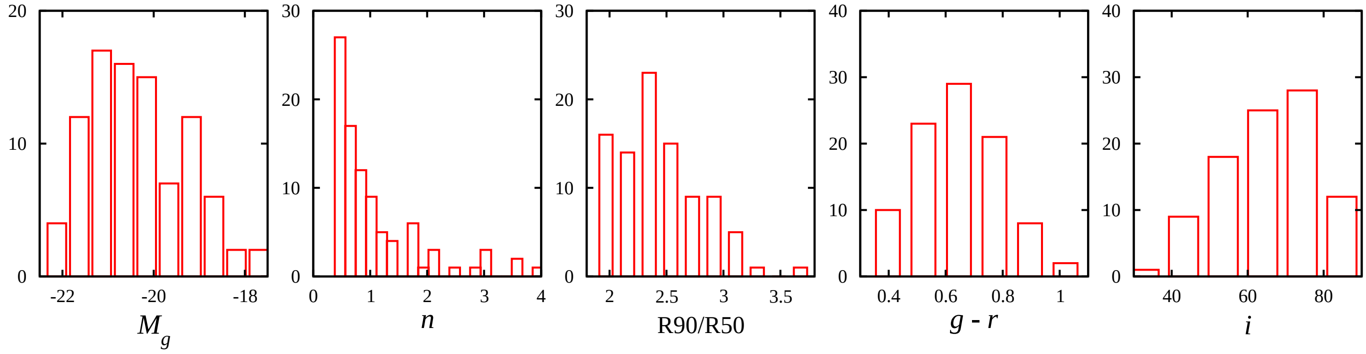

Figure 1. Frequency distribution of the variables that might affect the virial mass estimates for the $\mathbf{M_{nS}}$ sample. The approximately symmetrical cuts on the sample are made at -20.2, 0.8, 2.4, 0.6, 66° for magnitude, Sersic index, concentration, colour and inclination angle, respectively.

ies, the correlation is lower when the virial mass is obtained using the stars compared to when it is obtained by means of the gas. For red galaxies the opposite occurs. The method by which we obtained the virial mass does not seem to be of much consequence for the results above.

• When we take into account the inclination angle of the galaxy, we can see that for smaller inclination angles the slopes are greater than the slopes for larger inclination angles (see Table 6). We also find a clear difference in correlation coefficient and dispersion for samples with smaller inclination angles as compared with samples with larger inclination angles. Again, the method utilized to estimate the virial mass appears not to be of much significance.

The correlation of the fits is larger (lower dispersion) for galaxies with inclination angles $i > 66^o$ both when the velocity dispersion of the stars or the velocity dispersion of the gas is used. How the virial mass estimate was made was not significant.

• In general, the fits show a lower correlation (larger dispersion) when the galaxies are separated by luminosity values and larger correlation (lower dispersion) when the galaxies are separated by inclination angle values (see Tables 1-6 and Figures 2-8). In the latter case, the method utilised to make the virial mass estimate is not important, there are no significant differences whether the K factor is taken as a constant or is dependent on the Sersic index n, or the inclination angle. Neither are there important differences if we use the velocity dispersion of the stars or the gas velocity dispersion for the virial mass estimates.

The estimates of virial masses given in this paper must be considered carefully and the results and suggestions given above should be taken into account in terms of the method and parameters used to obtain a better determination of the virial masses. In all cases, the best calibrations for the virial mass are those for which the inclination angle is relatively high ($i > 66^o$). On the other hand, if you have samples of spiral galaxies with one of the following properties; relatively small Sersic index, relatively small concentration or blue color, it is more appropriate to use the virial mass estimate obtained with the gas velocity dispersion (H_α or the average velocity dispersion of the Balmer lines). For the opposite cases it is better to use the estimate of the virial mass obtained with the velocity dispersion of the stars.

9 CONCLUSIONS

Due to the difficulty of calculating the dynamical masses of LTGs and with the objective of using the enormous amount of data from the SDSS, in the present paper we calculate different estimates of the virial mass for LTGs. The assumptions we use include Newtonian dynamics, and virial equilibrium. The data used for calculation are provided by the SDSS dynamical information of each galaxy as represented by its stars and gas. The virial masses were calibrated by comparing them with a subsample of galaxies whose dynamical masses were obtained using their rotation curves. Moreover, we characterized the possible effects that different variables might have on the values of the virial mass estimates. Among the main variables that could affect the estimates of the virial mass we find the following: the scale factor K (see equation 8), the luminosity, the Sersic index n, the concentration index, the colour and the galaxy inclination angle.

The most important results that followed from the comparison of virial and dynamical masses, considering approximately symmetrical cuts in the variables mentioned above, are the following:

• In the case of cuts in luminosity no significant differences in the correlation coefficients of the fits for virial mass versus dynamical mass are found (see Table 1). We also find that the correlation coefficients are relatively low (relatively high dispersion), and that the method utilized to calculate the virial mass has no importance (see section 4.1). Neither are there important differences whether the stars or the gas are used in calculating the virial mass. From the above we conclude that galaxy luminosity is not an adequate variable to use to improve the determination of the virial mass.

• When we perform cuts in the Sersic index n, on the concentration index or on the colour $g - r$, the fits show a relatively high correlation in all cases (see Tables 2-4). We can see that for lower Sersic index, lower concentration and blue galaxies the slopes of the fits are lower than the slopes for greater Sersic index, greater concentration and red galaxies. It is interesting to note that if the Sersic index and/or the concentration are relatively low or if the color is blue, the correlation is higher if the velocity dispersion of the gas (H_α or the average velocity dispersion of the Balmer lines) are considered. For the opposite cases the correlation is higher if we consider the velocity dispersion of the stars. From this we may conclude that, as we might expect, for the smaller and bluer LTGs (dominated by the disk) the best indicator of the virial mass is the gas, while for larger and redder LTGs (dominated by the bulge), the best virial mass indicator is the stars. The method used to calculate the virial mass is of no consequence, in other words, there are no significant differences whether the virial mass is obtained with a constant K or if it is dependent on the Sersic n index or the inclination angle.

• In the case of cuts in the galactic inclination angle we find a highest correlation in the fits (lower dispersion) as compared to the variables discussed in the previous two items. We also can see that for smaller inclination angles the slopes are greater than the slopes for larger inclination angles. An evidently higher correlation appears for samples of galaxies with a larger inclination angle. In this case no significant differences due to the method used to obtain the virial mass is found. Neither are there significant differences whether the stars or the gas are used in the estimate of the virial mass. From this we may conclude that the better determined virial masses (using indistinctly the gas or the stars) are those for which the inclination angle is relatively high and that the method used for calculating this mass is of no importance, therefore, we may use either a constant K factor or a variable one without affecting substantially the estimate of the virial mass. The calibrations we used in this case are those presented in Table 6.

Considering these results and the calibration equation in Tables 1-6, we may conclude that the best calibrations for the virial masses of LTGs are those for galaxies with a relatively high inclination angle. If we have galaxies with relatively low inclination angles or we have samples of galaxies with heterogeneous properties one must take into consideration the size or colour of these galaxies through the use of the following variables: Sersic index n, concentration index or colour. For relatively smaller and bluer LTGs one must use the gas, while for LTGs that are relatively larger and redder one must use the stars.

If the reader wishes to perform their own virial mass estimates; they may use equation 1 and consider the calibration equations given in Tables 1-6 taking into consideration the properties of their sample and the advice given above.

ACKNOWLEDGEMENTS

We thank the Instituto de Astronomía y Meteorología (UdG, México) and Instituto de Astronomía (UNAM, México) for all the facilities provided for the realisation of this project. A. Nigoche-Netro acknowledges support from CONACyT and PRODEP (México). Eduardo de la Fuente thanks Colegio departamental de Física, authorities of CUCEI, Coordinación General Académica y de Innovación (CGAI-UDG), and the academic and administrative staff of the Institute for Cosmic Ray Research (ICRR), University of Tokyo (UTokyo), for authorization, acceptance, and support during his Sabbatical stay at ICRR in 2021. A. Ruelas-Mayorga thanks the Dirección General de Asuntos del Personal Académico, DGAPA at UNAM for financial support under project numbers PAPIIT IN103813 and PAPIIT IN102617. P. Lagos is supported in the form of work contract (DL 57/2016/CP1364/CT0010) funded by national funds through Fundação para a Ciência e Tecnologia (FCT), Portugal. We are indebted to Barbara Catinella who kindly made available the spiral galaxy rotation curves. Last but not least, we thank and acknowledge the comments made by an anonymous referee, which improved greatly the presentation of this paper.

Data availability. The data underlying this article are available in the article and in its online supplementary material.

REFERENCES

Akritas M. G., Bershady M. A., 1996, ApJ, 470, 706
Auger M. W., Treu T., Gavazzi R., Bolton A. S., Koopmans L. V. E., Marshall P. J., 2010, ApJ, 721, L163
Auger M. W., Treu T., Bolton A. S., Gavazzi R., Koopmans L. V. E., Marshall P. J., Bundy K., Moustakas L. A., 2011, VizieR Online Data Catalog, p. J/ApJ/705/1099
Baade W., 1944, ApJ, 100, 137
Babcock H. W., 1939, Lick Observatory Bulletin, 498, 41
Bertin G., Saglia R. P., Stiavelli M., 1992, ApJ, 384, 423
Bertola F., Bettoni D., Rusconi L., Sedmak G., 1984, AJ, 89, 356
Bica E., Alloin D., 1986, A&A, 162, 21
Blanton M. R., et al., 2003, ApJ, 594, 186
Bolton A. S., Burles S., Schlegel D. J., Eisenstein D. J., Brinkmann J., 2004, AJ, 127, 1860
Bolton A. S., Burles S., Koopmans L. V. E., Treu T., Moustakas L. A., 2005, ApJ, 624, L21
Bolton A. S., Burles S., Koopmans L. V. E., Treu T., Moustakas L. A., 2006, ApJ, 638, 703
Bolton A. S., Burles S., Koopmans L. V. E., Treu T., Gavazzi R., Moustakas L. A., Wayth R., Schlegel D. J., 2008, ApJ, 682, 964
Brainerd T. G., Blandford R. D., Smail I., 1996, in American Astronomical Society Meeting Abstracts #188. p. 13.02

Bruzual A. G., 1983, ApJ, 273, 105
Burbidge E. M., Burbidge G. R., 1975, in Sandage A., Sandage M., Kristian J., eds, , Galaxies and the Universe. p. 81
Burbidge E. M., Burbidge G. R., Fish R. A., 1961a, ApJ, 133, 393
Burbidge E. M., Burbidge G. R., Fish R. A., 1961b, ApJ, 133, 1092
Burbidge E. M., Burbidge G. R., Fish R. A., 1961c, ApJ, 134, 251
Cappellari M., et al., 2006, MNRAS, 366, 1126
Catinella B., Haynes M. P., Giovanelli R., 2005, AJ, 130, 1037
Catinella B., Haynes M. P., Giovanelli R., 2007, AJ, 134, 334
Cayatte V., Kotanyi C., Balkowski C., van Gorkom J. H., 1994, AJ, 107, 1003
Chabrier G., 2003, PASP, 115, 763
Conroy C., 2013, ARA&A, 51, 393
Cooper M. C., Gallazzi A., Newman J. A., Yan R., 2010, MNRAS, 402, 1942
Courteau S., 1997, AJ, 114, 2402
Courteau S., Sohn Y.-J., 2003, in Bender R., Renzini A., eds, The Mass of Galaxies at Low and High Redshift. p. 204 (arXiv:astro-ph/0202267), doi:10.1007/10899892_50
Courteau S., et al., 2014, Rev. Mod. Phys., 86, 47
De Lucia G., et al., 2007, MNRAS, 374, 809
Faber S. M., 1972, A&A, 20, 361
Faber S. M., Gallagher J. S., 1979, ARA&A, 17, 135
Fahlman G., Kaiser N., Squires G., Woods D., 1994, ApJ, 437, 56
Féron C., Hjorth J., McKean J. P., Samsing J., 2009, ApJ, 696, 1319
Fich M., Tremaine S., 1991, ARA&A, 29, 409
Fisher D., 1997, AJ, 113, 950
Gavazzi R., Treu T., Rhodes J. D., Koopmans L. V. E., Bolton A. S., Burles S., Massey R. J., Moustakas L. A., 2007, ApJ, 667, 176
Graham A. W., Driver S. P., Petrosian V., Conselice C. J., Bershady M. A., Crawford S. M., Goto T., 2005, AJ, 130, 1535
Greggio L., Renzini A., 2011, Stellar Populations. A User Guide from Low to High Redshift
Hyde J. B., Bernardi M., 2009, MNRAS, 394, 1978
Isobe T., Feigelson E. D., Akritas M. G., Babu G. J., 1990, ApJ, 364, 104
Jørgensen I., Franx M., Kjaergaard P., 1995a, MNRAS, 273, 1097
Jørgensen I., Franx M., Kjaergaard P., 1995b, MNRAS, 276, 1341
Kaiser N., Squires G., 1993, ApJ, 404, 441
Kapteyn J. C., van Rhijn P. J., 1922, Bull. Astron. Inst. Netherlands, 1, 37
Keeton C. R., 2001, ApJ, 561, 46
King I. R., Minkowski R., 1966, ApJ, 143, 1002
Knapp G. R., Turner E. L., Cunniffe P. E., 1985, AJ, 90, 454
Koopmans L. V. E., Treu T., Bolton A. S., Burles S., Moustakas L. A., 2006, ApJ, 649, 599
Kroupa P., 2001, MNRAS, 322, 231
Lagattuta D. J., et al., 2010, ApJ, 716, 1579
Lallemand A., Duchesne M., Walker M. F., 1960, PASP, 72, 283
Loewenstein M., White Raymond E. I., 1999, ApJ, 518, 50
MacArthur L. A., Courteau S., Bell E., Holtzman J. A., 2004, ApJS, 152, 175
MacArthur L. A., González J. J., Courteau S., 2009, MNRAS, 395, 28
Mathewson D. S., Ford V. L., Buchhorn M., 1992, ApJS, 81, 413
Mayall N. U., 1950, Publ. Obs. Univ. Michigan, 10, 19
McKay T. A., et al., 2002, ApJ, 571, L85
Minkowsky R., 1954, Carnegie Inst. Yearbook, 53, 26
Minkowsky R., 1961, IAU Symposium No. 15 ed. G. C. McVittie, p. 112
Miyamoto M., Nagai R., 1975, PASJ, 27, 533
Mocz P., Green A., Malacari M., Glazebrook K., 2012, MNRAS, 425, 296
Morganti R., et al., 2006, MNRAS, 371, 157
Newton E. R., Marshall P. J., Treu T., Auger M. W., Gavazzi R., Bolton A. S., Koopmans L. V. E., Moustakas L. A., 2011, ApJ, 734, 104
Nigoche-Netro A., Ruelas-Mayorga A., Franco-Balderas A., 2008, A&A, 491, 731
Nigoche-Netro A., Aguerri J. A. L., Lagos P., Ruelas-Mayorga A., Sánchez L. J., Machado A., 2010, A&A, 516, A96
Nigoche-Netro A., Ruelas-Mayorga A., Lagos P., Ramos-Larios G., Kehrig C., Kemp S. N., Montero-Dorta A. D., González-Cervantes J., 2015, MNRAS, 446, 18
O'Connell R. W., 1976, ApJ, 206, 370
Oort J. H., 1926, The Observatory, 49, 302
Oort J. H., 1932a, Bull. Astron. Inst. Netherlands, 6, 249
Oort J. H., 1932b, Bull. Astron. Inst. Netherlands, 6, 289
Opik E., 1922, ApJ, 55, 406
Padmanabhan N., et al., 2004, New Astron., 9, 329
Pease F. G., 1918, Proceedings of the National Academy of Science, 4, 21
Pickles A. J., 1985, ApJ, 296, 340
Poveda A., 1958, Boletin de los Observatorios Tonantzintla y Tacubaya, 2, 3
Prada F., et al., 2003, ApJ, 598, 260
Renzini A., Voli M., 1981, A&A, 94, 175
Roberts M. S., Whitehurst R. N., 1975, ApJ, 201, 327
Rubin V. C., Ford W. K. J., 1970, in Becker W., Kontopoulos G. I., eds, Vol. 38, The Spiral Structure of our Galaxy. p. 61
Rubin V. C., Burstein D., Ford W. K. J., Thonnard N., 1985, ApJ, 289, 81
Sage L. J., Welch G. A., Young L. M., 2007, ApJ, 657, 232
Saglia R. P., Bertin G., Stiavelli M., 1992, ApJ, 384, 433
Salpeter E. E., 1955, ApJ, 121, 161
Sandage A., 1986, A&A, 161, 89
Sarzi M., et al., 2006, MNRAS, 366, 1151
Scalo J. M., 1986, Fundamentals Cosmic Phys., 11, 1
Scheiner J., 1899, ApJ, 9, 149
Schneider P., 2006, in Meylan G., Jetzer P., North P., Schneider P., Kochanek C. S., Wambsganss J., eds, Saas-Fee Advanced Course 33: Gravitational Lensing: Strong, Weak and Micro. pp 1–89
Sersic J. L., 1968, Atlas de Galaxias Australes
Simon J. D., Bolatto A. D., Leroy A., Blitz L., 2003, ApJ, 596, 957
Simon J. D., Bolatto A. D., Leroy A., Blitz L., Gates E. L., 2005, ApJ, 621, 757
Slipher V. M., 1914, Popular Astronomy, 22, 19
Sofue Y., Rubin V., 2001, ARA&A, 39, 137
Spekkens K., Sellwood J. A., 2007, ApJ, 664, 204
Spinrad H., Taylor B. J., 1971, ApJS, 22, 445
Sygnet J. F., Tu H., Fort B., Gavazzi R., 2010, A&A, 517, A25
Tinsley B. M., 1972, A&A, 20, 383
Tinsley B. M., Gunn J. E., 1976, ApJ, 203, 52
Treu T., 2010, ARA&A, 48, 87
Treu T., Koopmans L. V., Bolton A. S., Burles S., Moustakas L. A., 2006, ApJ, 640, 662
Treu T., Gavazzi R., Gorecki A., Marshall P. J., Koopmans L. V. E., Bolton A. S., Moustakas L. A., Burles S., 2009, ApJ,

692, 1690
Treu T., Dutton A. A., Auger M. W., Marshall P. J., Bolton A. S., Brewer B. J., Koo D. C., Koopmans L. V. E., 2011, MNRAS, 417, 1601
Tyson J. A., Valdes F., Jarvis J. F., Mills A. P. J., 1984, ApJ, 281, L59
Tyson J. A., Valdes F., Wenk R. A., 1990, ApJ, 349, L1
Walcher J., Groves B., Budavári T., Dale D., 2011, Ap&SS, 331, 1
York D. G., et al., 2000, AJ, 120, 1579
Young L. M., et al., 2011, MNRAS, 414, 940
de Vaucouleurs G., 1963, ApJ, 137, 720
di Serego Alighieri S., et al., 2007, A&A, 474, 851

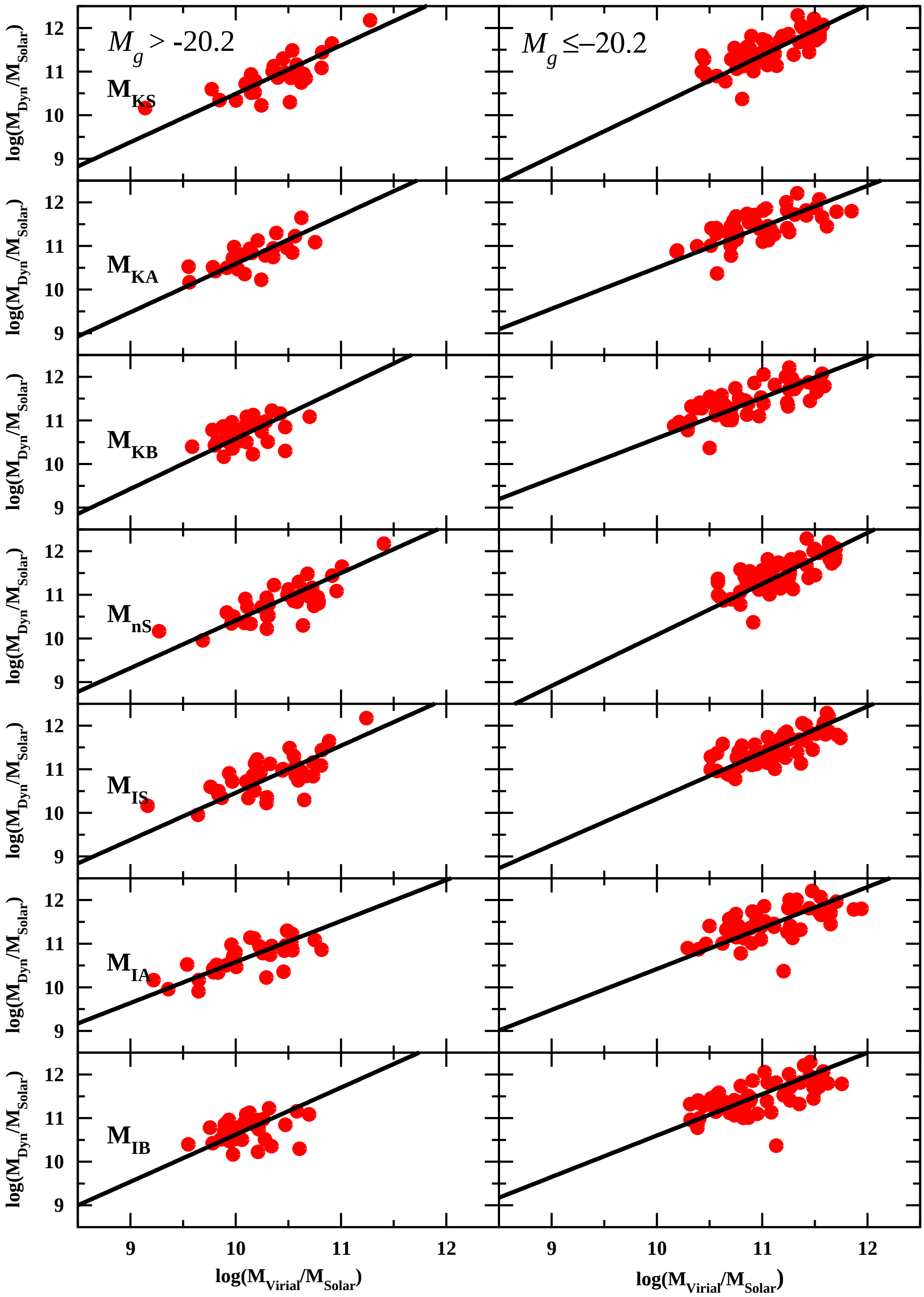

Figure 2. Distribution of the logarithmic difference between virial and dynamical mass for two absolute magnitude cuts ($M_g > -20.2$, $M_g \leqslant -20.2$) and different virial mass estimations. Black continuous lines are BCES$_{Bis}$ fits

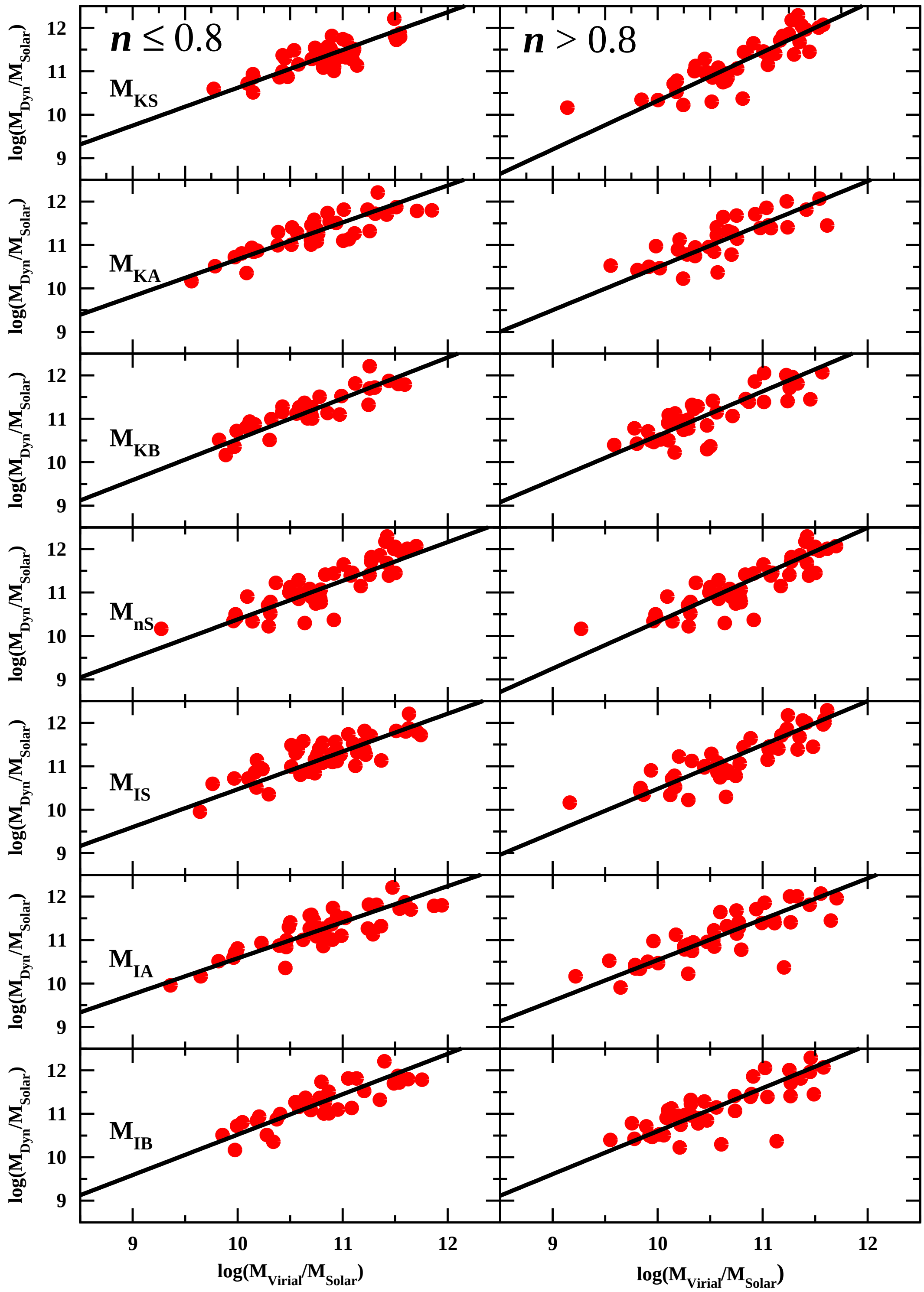

Figure 3. Distribution of the logarithmic difference between virial and dynamical mass for two Sersic index cuts ($n \leqslant 0.8$, $n > 0.8$) and different virial mass estimations. Black continuous lines are BCES$_{Bis}$ fits

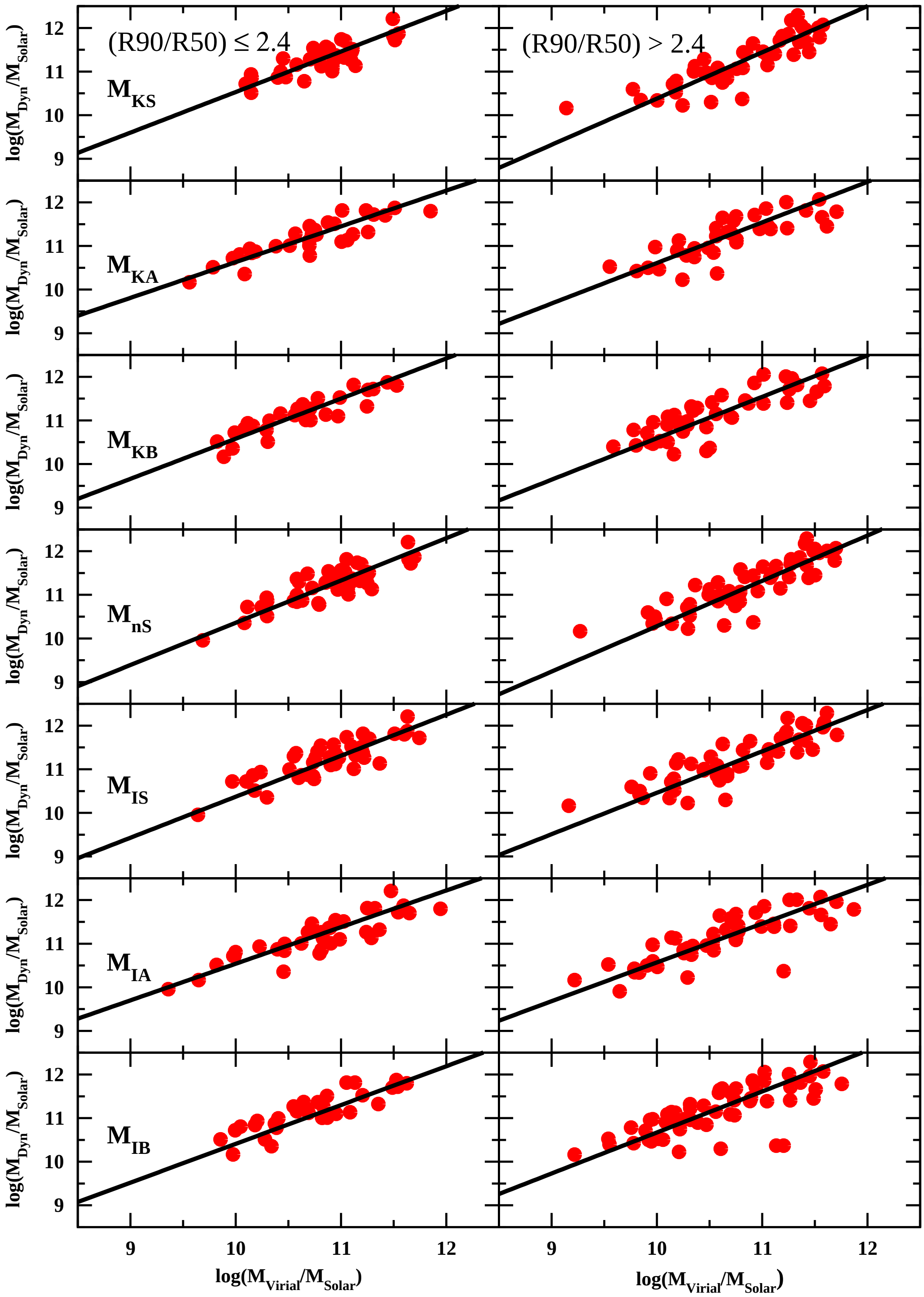

Figure 4. Distribution of the logarithmic difference between virial and dynamical mass for two concentration index cuts ($(R90/R50) \leqslant 2.4$, $(R90/R50) > 2.4$) and different virial mass estimations. Black continuous lines are BCES$_{Bis}$ fits

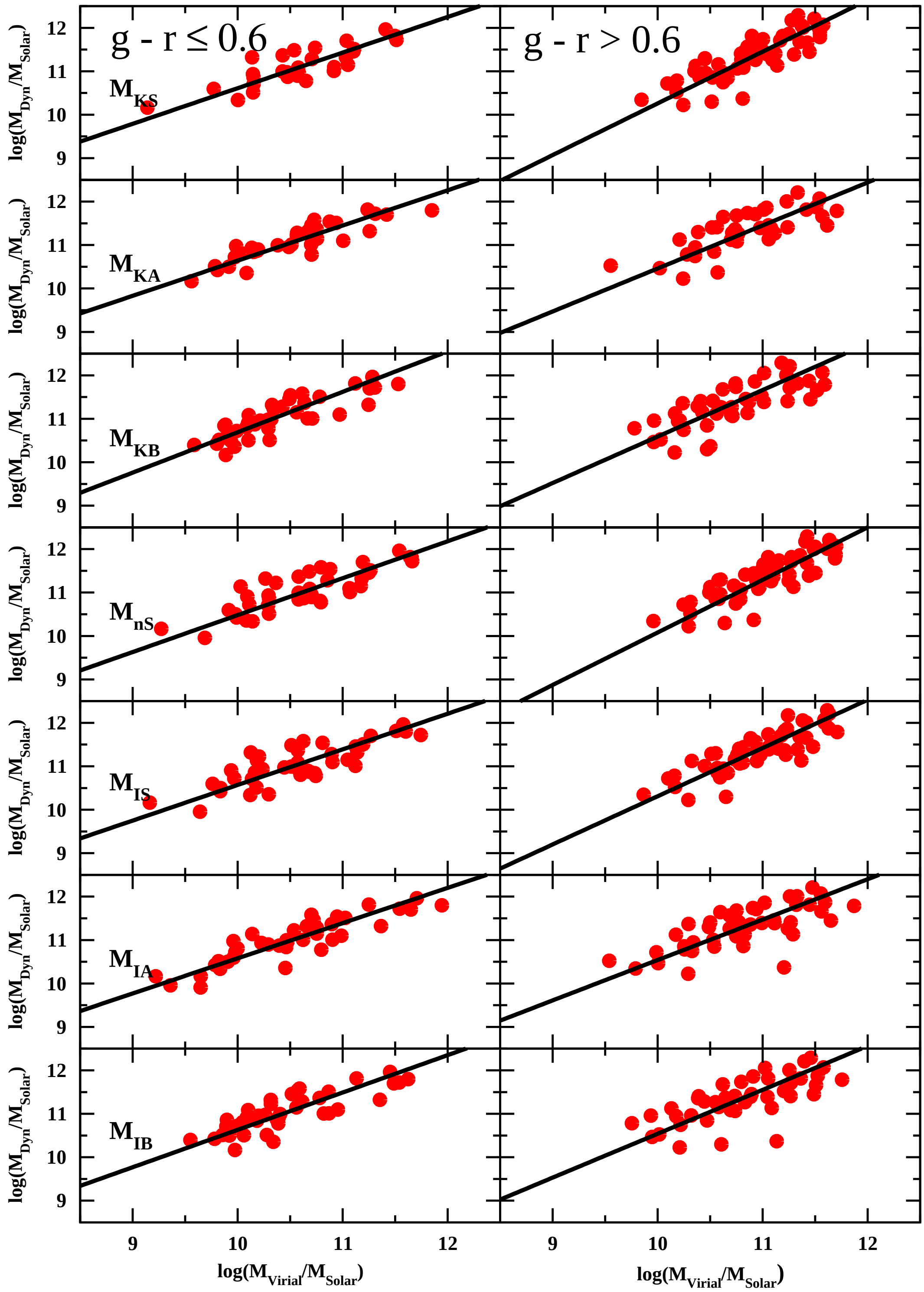

Figure 5. Distribution of the logarithmic difference between virial and dynamical mass for two colour cuts ($g - r \leqslant 0.6$, $g - r > 0.6$) and different virial mass estimations. Black continuous lines are BCES_{Bis} fits

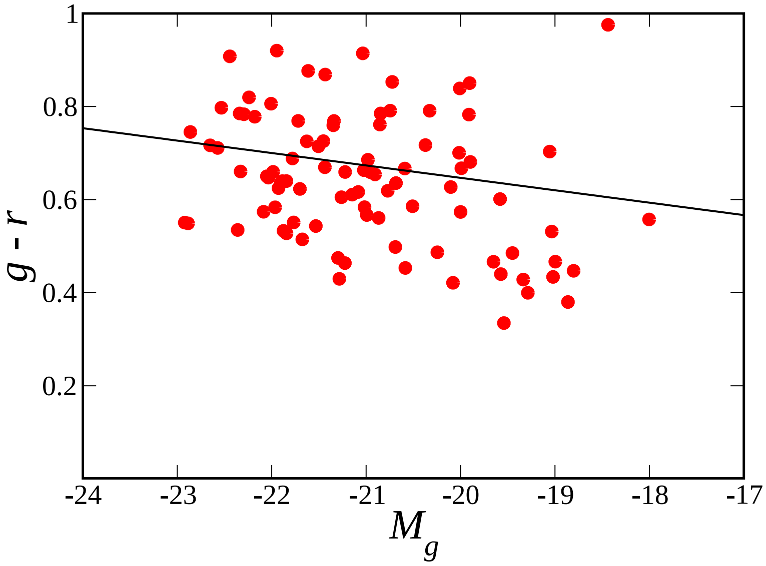

Figure 6. Colour-magnitude diagram of the $\mathbf{M_{nS}}$ sample. The black line represents the limit of the red sequence according to Cooper et al. (2010).

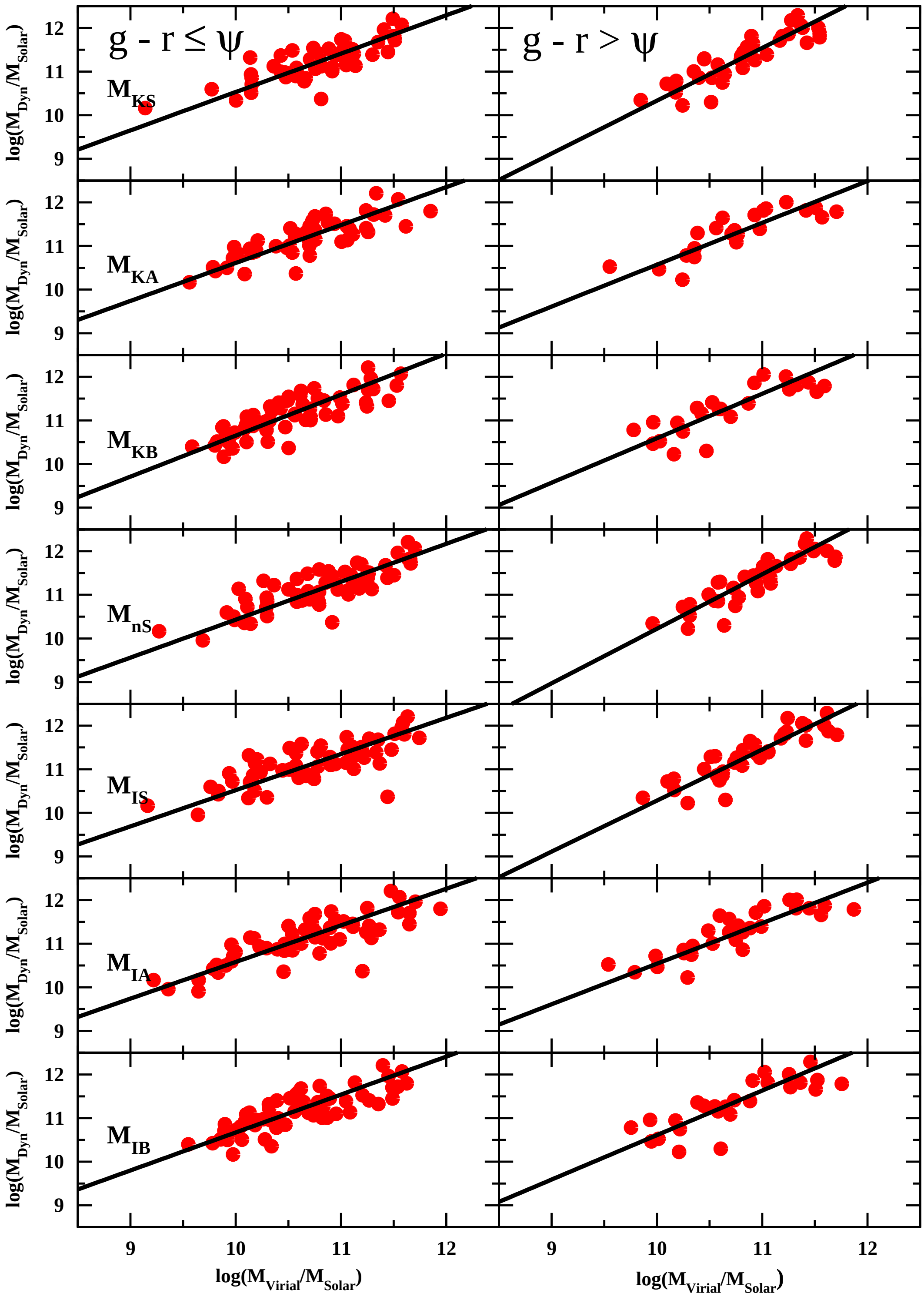

Figure 7. Distribution of the logarithmic difference between virial and dynamical mass for two colour cuts considering the Red Sequence limit ($\psi = -0.02667 M_r + 0.11333$; Cooper et al. 2010) and different virial mass estimations. Black continuous lines are BCES_{Bis} fits.

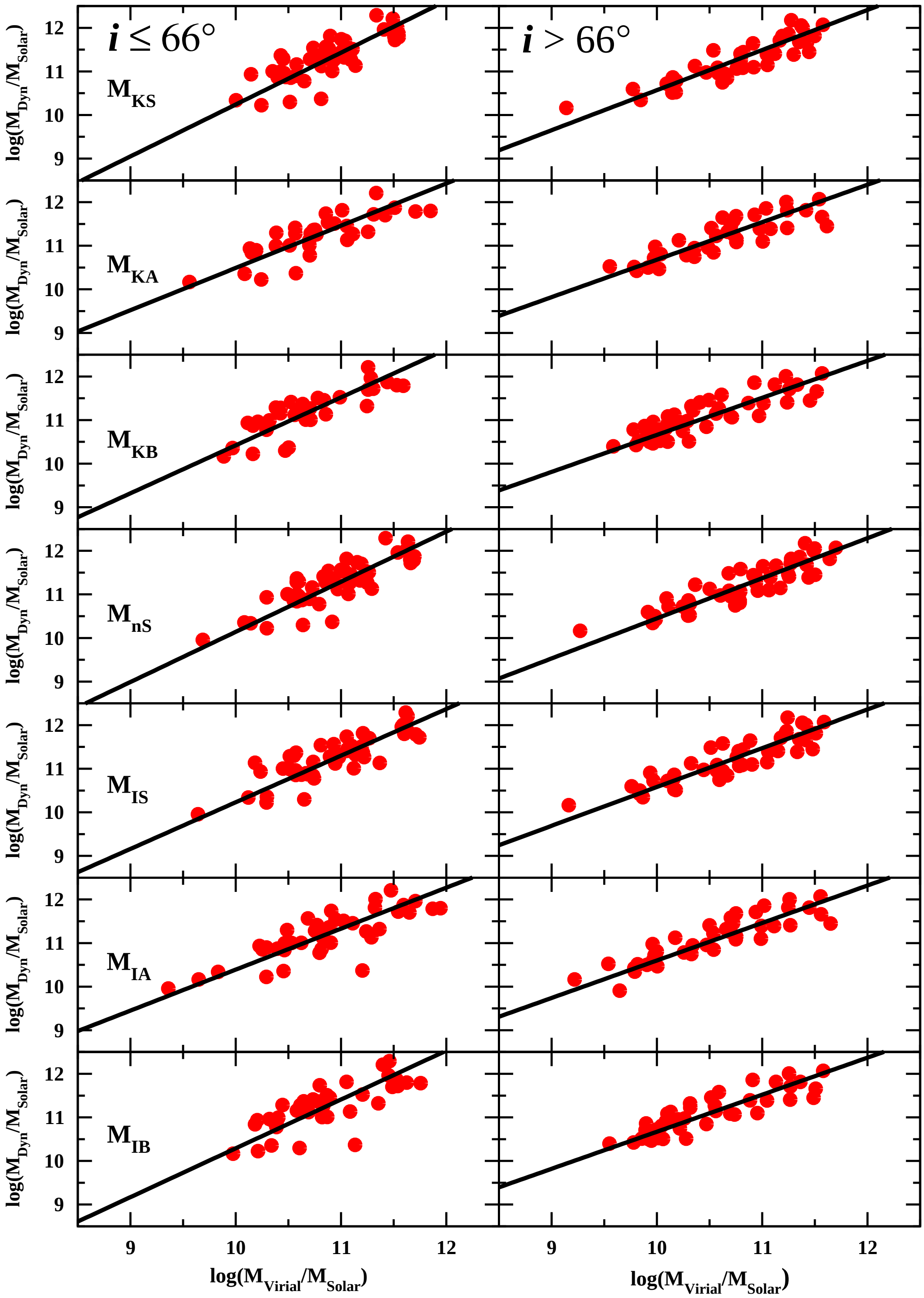

Figure 8. Distribution of the logarithmic difference between virial and dynamical mass for two inclination angle cuts ($i \leqslant 66^o$, $i > 66^o$) and different virial mass estimations. Black continuous lines are BCES_{Bis} fits

10 APPENDIX A

In Table A.1 we show the virial masses, and some parameters involved in the analysis of this work, of a sub-sample of 145 LTGs from SDSS DR16 with information in Catinella et al. (2005). The virial masses were obtained following the procedure described in section 4. In column 1 we find the galaxy name in SDSS DR16. In column 2 we find the redshift from SDSS DR16. In column 3 we find the absolute magnitude in the g filter, estimated using the apparent magnitude from the SDSS DR16. In column 4 we find the colour $g-r$ from the SDSS DR16. In columns 5 and 6 we find the ratio of the Petrosian radii R90 and R50 from the SDSS DR16 in the g and r filters respectively. In columns 7 and 8 we find the Sersic index n, in the g and r filters respectively, estimated using the procedure described in section 6. In column 9 and 10 we find the galactic inclination angles, in the g and r filters respectively, estimated using equation 1 from section 4.1. Finally, in columns 11, 12, 13, 14, 15, 16, and 17 we find the logarithmic virial masses $\mathbf{M_{KS}}$, $\mathbf{M_{KA}}$, $\mathbf{M_{KB}}$, $\mathbf{M_{nS}}$, $\mathbf{M_{IS}}$, $\mathbf{M_{IA}}$, and $\mathbf{M_{IB}}$ respectively. The entire catalogue of virial masses of 126 699 LTGs from the SDSS (see section 2) with the same structure of Table A.1, can be found in electronic form in the following link:

It is very important to remark that the previously mentioned masses must be corrected, depending on the necessities of the reader, using Tables 1-6 from section 7 and the advice given in section 9.

In Table A.2 we show the dynamical masses of a subsample of 145 LTGs from Catinella et al. (2005) with photometric and/or spectroscopic information in the SDSS DR16. The dynamical masses were obtained using the rotation curves from Catinnella et al. 2005 as described in section 5. In column 1 we find the galaxy name in the Arecibo General Catalog (AGC). In Column 2 we show other names of the galaxy (NGC, IC, CGCG or MCG). In column 3 we find the SDSS DR16 name. In columns 4 and 5 we find the right ascension and declination, respectively. Finally, in column 6 we find the dynamical mass in solar masses.

Table A1. Virial masses of a subsample of 145 LTGs from Catinella et al. (2005) with photometric and/or spectroscopic information in the SDSS DR16.

SDSS DR16	z	M_g	$g-r$	$R50/R90_g$	$R50/R90_r$	n_g	n_r	i_g	i_r	$\mathbf{M_{KS}}$	$\mathbf{M_{KA}}$	$\mathbf{M_{KB}}$	$\mathbf{M_{nS}}$	$\mathbf{M_{IS}}$	$\mathbf{M_{IA}}$	$\mathbf{M_{IB}}$
1237653653447180545	0.01872±0.00002	-19.05±0.0065	0.08504±0.0085	2.595±0.2061	2.665±0.0945	0.9331±0.3671	1.068±0.1989	78.47±0.6191	84.43±1.043	10.18±0.0953	10.28±0.0297	9.779±0.0793	10.31±0.0953	10.16±0.0400	10.26±0.0125	9.756±0.0333
1237652629638873182	0.03893±0.00002	-20.15±0.0050	0.6190±0.0066	2.328±0.0655	2.391±0.0434	0.5865±0.0589	0.6482±0.0462	80.71±1.326	83.48±1.142	10.54±0.0799	10.25±0.0453	10.16±0.0540	10.68±0.0799	10.51±0.0336	10.23±0.0191	10.13±0.0227
1237652947456360495	0.01312±0.00001	-20.95±0.0032	0.7691±0.0045	2.956±0.2660	3.013±0.3245	1.937±1.075	2.181±1.480	6824±0.2975	68.23±0.2784	11.19±0.0112	11.42±0.0643	11.33±0.0495	11.28±0.0112	11.22±0.0045	11.45±0.0254	11.36±0.0195
1237652947993624616	0.02032±0.00001	-19.86±0.0041	0.3786±0.0059	-	-	0.3278±11.87	0.3402±16.78	49.55±0.5539	49.83±0.5344	9.062±0.6737	9.975±0.0180	9.957±0.0236	9.219±0.6737	9.264±0.2182	10.18±0.0059	10.16±0.0077
1237652900753244294	0.01925±0.00001	-18.89±0.0042	0.3997±0.0059	2.592±0.1168	2.586±0.1665	0.9280±0.2066	0.9170±0.2899	80.57±0.9919	80.70±1.093	9.856±0.2327	9.808±0.0097	9.802±0.0140	9.989±0.2327	9.834±0.0975	9.786±0.0042	9.780±0.0059
1237652900753244175	0.01911±0.00001	-20.56±0.0028	0.8687±0.0038	3.147±0.6629	3.246±0.7332	2.886±3.976	3.543±5.347	71.29±0.3562	70.91±0.3030	11.04±0.0137	10.98±0.0309	10.87±0.0295	11.08±0.0137	11.06±0.0055	10.99±0.0124	10.88±0.0119
1237652900753244328	0.00448±0.00001	-17.15±0.0079	0.1221±0.0109	2.317±0.0941	2.276±2.277	0.5770±0.0821	0.5431±1.775	90	90	10.02±0.4501	-	-	10.17±0.4501	9.983±0.1924	9.731±0.0090	-
1237652947993952343	0.02021±0.00001	-18.91±0.0073	0.4281±0.0104	1.927±0.0354	1.971±0.0332	0.3720±0.0097	0.3851±0.0105	38.76±0.9533	39.21±0.9607	9.927±0.2006	10.09±0.0322	9.971±0.0427	10.08±0.2006	10.30±0.0536	10.45±0.0088	10.34±0.0115
1237663782593822774	0.01798±0.00001	-19.32±0.0039	0.5806±0.0053	2.057±0.0314	2.099±0.0241	0.4162±0.0129	0.4349±0.0113	61.93±0.5195	62.40±0.4355	10.07±0.0896	10.23±0.0077	10.22±0.0091	10.22±0.0896	10.14±0.0337	10.30±0.0030	10.30±0.0035
1237666338115027075	0.01908±0.00002	-18.99±0.0058	0.9062±0.0082	2.450±0.0968	2.693±0.1221	0.7160±0.1200	1.129±0.2746	78.52±0.7862	77.97±0.5351	9.464±0.3898	10.02±0.0276	9.963±0.0351	9.597±0.3898	9.449±0.1621	10.01±0.0115	9.948±0.0146
1237663783130759334	0.01934±0.00001	-17.98±0.0074	0.3800±0.0117	2.382±0.1256	2.502±0.1110	0.6383±0.1302	0.7855±0.1572	48.55±1.102	46.46±1.240	9.922±0.3583	9.629±0.0241	9.762±0.0247	10.06±0.3583	10.15±0.1122	9.860±0.0079	9.993±0.0081
1237666338115092762	0.06611±0.00003	-21.08±0.0053	0.6229±0.0069	1.939±0.0351	2.004±0.0290	0.3756±0.0099	0.3958±0.0101	44.03±0.8335	47.09±0.5849	10.95±0.0608	10.03±0.3792	10.39±0.1678	11.10±0.0608	11.21±0.0185	10.29±0.1150	10.65±0.0509
1237663783130824820	0.06646±0.00002	-20.30±0.0076	0.6856±0.0094	2.310±0.1086	2.452±0.1019	0.5709±0.0929	0.7188±0.1270	90	90	10.80±0.1073	10.72±0.0297	10.59±0.0338	10.94±0.1073	10.76±0.0458	10.69±0.0128	10.55±0.0146
1237666338652618892	0.01771±0.00001	-18.54±0.0057	0.2947±0.0086	2.0349±0.0491	2.083±0.0443	0.4073±0.0189	0.4273±0.0197	60.80±0.7683	60.09±0.8447	-	9.560±0.0943	9.887±0.0682	-	10.76	9.648±0.0349	9.975±0.0252
1237663784205680908	0.03935±0.00002	-19.59±0.0073	0.8128±0.0092	2.571±0.1674	2.626±0.3213	0.8923±0.2814	0.9894±0.6159	82.24±1.885	81.98±1.317	10.61±0.0629	10.72±0.0568	10.22±0.0848	10.74±0.0629	10.58±0.0265	10.70±0.0239	10.19±0.0357
1237666339190472839	0.00581±0.00003	-16.79±0.0247	0.3531±0.0377	2.169±0.1136	2.229±0.0515	0.4707±0.0653	0.5086±0.0352	74.50±0.7108	76.32±1.600	9.917±0.2808	-	-	10.06±0.2808	9.912±0.1154	9.537±0.0653	-
1237663784206270641	0.01266±0.00002	-18.88±0.0101	0.3543±0.0140	2.027±0.0325	2.119±0.0272	0.4043±0.0122	0.4444±0.0135	68.37±0.6463	67.69±0.6588	9.7200±0.2465	9.056±0.2469	9.696±0.1062	9.873±0.2465	9.752±0.0971	9.088±0.0972	9.728±0.0418
1237666338116993064	0.02712±0.00001	-21.86±0.0027	0.7110±0.0037	2.305±0.0249	2.457±0.0363	0.5666±0.021	0.7259±0.0459	57.48±0.3404	52.30±0.2993	11.49±0.0159	11.33±0.0688	11.26±0.0609	11.64±0.0159	11.63±0.0056	11.47±0.0239	11.40±0.0212
1237663783132790881	0.00662±0.00001	-10.29±0.1984	0.5014±0.2355	-	-	-	-	60	61.64	8.892±0.2247	-	-	9.049±0.2247	8.882±0.1312	8.255±0.1026	-
1237657189840584856	0.02590±0.00001	-20.05±0.0039	0.6355±0.0052	2.658±0.1479	2.783±0.1539	1.053±0.3060	1.355±0.4258	74.23±0.4140	73.70±0.4344	10.67±0.0357	10.54±0.0125	10.47±0.0135	10.79±0.0357	10.68±0.0146	10.54±0.0052	10.47±0.0056
1237663782597034125	-	-	-	-	-	-	-	81	81	-	-	-	-	-	-	-
1237663782597099527	0.01547±0.00001	-19.92±0.0046	0.5857±0.0064	2.726±0.1654	2.907±0.1503	1.206±0.4011	1.748±0.5467	76.79±0.1545	74.35±0.3652	10.58±0.0261	8.576±0.2134	10.11±0.0266	10.69±0.0261	10.57±0.0108	8.570±0.0877	10.10±0.0110
1237657069546831898	0.01632±0.00001	-20.29±0.0032	0.6588±0.0045	3.129±0.6831	3.251±0.6621	2.778±3.951	3.581±4.878	70.42±0.1723	68.24±0.2631	10.76±0.0149	9.511±0.0005	10.72±0.0733	10.79±0.0149	10.78±0.0059	9.535±0.0005	10.74±0.0291
1237678880495894618	-	-	-	-	-	-	-	65	65	-	-	-	-	-	-	-
1237653652921057594	0.02639±0.00001	-21.13±0.0029	0.6943±0.0040	2.963±0.4245	3.118±0.5008	1.967±1.744	2.718±2.835	71.33±0.4067	71.91±0.3381	11.12±0.0171	11.18±0.0887	11.02±0.0701	11.19±0.0171	11.13±0.0069	11.19±0.0358	11.03±0.0283
1237652900223909957	0.01790±0.00001	-20.54±0.0027	0.6106±0.0038	2.542±0.0282	2.576±0.0246	0.8446±0.0442	0.9006±0.0419	58.92±0.2779	59.39±0.2631	10.57±0.0168	10.19±0.0295	10.29±0.0209	10.70±0.0168	10.67±0.0062	10.29±0.0108	10.39±0.0077
1237663783676477669	0.02131±0.00001	-21.03±0.0029	0.9200±0.0038	1.936±0.0116	2.045±0.0288	0.3745±0.0033	0.4114±0.0114	35.45±0.5561	48.36±0.4421	10.90±0.0132	11.01±0.0328	10.74±0.0337	11.05±0.0132	11.21±0.0039	11.32±0.0094	11.05±0.0097
1237657070628503722	0.07550±0.00001	-21.39±0.0057	0.6914±0.0074	2.332±0.1262	2.460±0.1266	0.5899±0.1145	0.7288±0.1610	78.25±1.1577	77.89±0.8764	11.39±0.0444	-	-	11.53±0.0444	11.37±0.0185	11.30±0.0061	-
1237657584951034038	0.02349±0.00002	-19.31±0.0065	0.7005±0.0085	2.435±0.0564	2.655±0.1065	0.6974±0.0672	1.047±0.2188	79.35±1.253	78.36±0.8041	10.64±0.1297	10.36±0.0352	10.19±0.0465	10.78±0.1297	10.63±0.0541	10.34±0.0147	10.18±0.0194
1237663783142096968	0.02164±0.00001	-21.20±0.0035	0.6398±0.0048	2.478±0.0817	2.622±0.0953	0.7519±0.1088	0.9832±0.1813	69.79±0.4075	67.23±0.3277	11.12±0.0238	11.24±0.0060	11.24±0.0058	11.26±0.0238	11.15±0.0094	11.27±0.0025	11.27±0.0024
1237663783142228130	0.02189±0.00001	-19.13±0.0064	0.4399±0.0089	2.256±0.0923	2.367±0.0798	0.5279±0.0681	0.6239±0.0797	74.13±0.9235	72.58±0.6751	9.964±0.1655	9.974±0.0165	9.990±0.0191	10.11±0.1655	9.968±0.0674	9.978±0.0068	9.995±0.0079
1237663783142228165	-	-	-	-	-	-	-	68	68	-	-	-	-	-	-	-
1237657584951230617	0.02342±0.00001	-20.25±0.0043	0.6541±0.0058	2.312±0.0315	2.451±0.0496	0.5726±0.0271	0.7177±0.0617	78.693±0.5700	79.36±0.4983	10.79±0.0593	10.52±0.0236	10.41±0.0290	10.94±0.0593	10.78±0.0247	10.50±0.0099	10.39±0.0121
1237652900767268885	0.01730±0.00002	-20.31±0.0051	0.5606±0.0071	1.877±0.2926	1.999±0.2754	0.3596±0.0678	0.3941±0.0947	47.69±0.3971	50.68±0.3523	10.48±0.0777	10.19±0.0225	10.16±0.0277	10.63±0.0777	10.68±0.0250	10.40±0.0073	10.37±0.0089
1237663784217149628	0.00948±0.00002	-17.90±0.0135	0.3286±0.0366	2.204±0.0996	2.221±0.0500	0.4923±0.0634	0.5029±0.0333	76.72±1.524	79.60±4.546	10.34±0.2130	-	-	10.49±0.2130	10.32±0.0887	9.659±0.0403	-
1237666300018229273	0.02267±0.00001	-20.58±0.0040	0.6019±0.0055	2.620±0.2286	2.694±0.0514	0.9781±0.4319	1.133±0.1228	76.40±0.5634	78.34±0.4922	10.14±0.1150	10.67±0.0498	10.33±0.0713	10.26±0.1150	10.13±0.0476	10.66±0.0207	10.32±0.0954
1237649964066406405	0.01891±0.00001	-21.55±0.0028	0.7851±0.0038	2.598±0.0687	2.699±0.0967	0.9387±0.1232	1.142±0.2203	73.63±0.3427	70.24±0.3288	11.37±0.0140	8.925±0.7590	11.01±0.0641	11.50±0.0140	11.38±0.0057	8.936±0.3064	11.02±0.0259
1237653588477411643	-	-	-	-	-	-	-	66	66	-	-	-	-	-	-	-
1237660764834103400	0.01392±0.00001	-18.58±0.0060	0.6762±0.0088	2.366±68.41	2.456±70.84	0.6226±68.08	0.7238±89.2227	78.02±0.5516	70	9.437±0.8147	9.152±0.1715	9.965±0.0573	9.580±0.8147	9.408±0.3442	9.123±0.0725	9.936±0.0242
1237664837535858925	-	-	-	-	-	-	-	50	50	-	-	-	-	-	-	-
1237667782809223472	-	-	-	-	-	-	-	72	72	-	-	-	-	-	-	-
1237667782809223502	0.07771±0.00001	-20.69±0.0069	0.6491±0.0089	2.173±0.0995	2.387±0.0791	0.4733±0.0579	0.6440±0.0832	84.81±2.920	84.15±2.1211	10.67±0.1342	11.15±0.0176	11.10±0.0183	10.81±0.1342	10.64±0.0568	11.12±0.0076	11.07±0.0079
1237661086957568117	0.07600±0.00002	-20.82±0.0078	0.4747±0.0102	2.366±0.2197	2.457±0.1390	0.6227±0.2187	0.7250±0.1755	82.93±3.013	82.03±2.118	10.65±0.2132	10.73±0.0484	10.62±0.0556	10.79±0.2132	10.63±0.0898	10.70±0.0205	10.59±0.0235
1237664092898852896	0.02610±0.00001	-21.39±0.0029	0.6472±0.0040	2.622±0.3894	2.765±0.3534	0.9824±0.7398	1.307±0.9389	72.94±0.3811	70.60±0.3792	11.58±0.0147	11.54±0.0624	11.57±0.0503	11.70±0.0147	11.59±0.0060	11.55±0.0252	11.58±0.0203
1237654601019686930	0.01299±0.00001	-21.42±0.0034	0.8196±0.0048	2.938±0.0886	2.996±0.0976	1.867±0.3449	2.105±0.4292	44.53±0.2229	44.09±0.2119	11.34±0.0105	10.58±0.0663	11.18±0.0469	11.42±0.0105	11.62±0.0032	10.86±0.0197	11.46±0.0139
1237664093438214204	-	-	-	-	-	-	-	65	65	-	-	-	-	-	-	-
1237660412649865229	0.00492±0.00001	-17.67±0.0187	0.225±0.0209	2.230±0.0183	2.238±0.0407	0.5096±0.0126	0.5151±0.0286	40.43±1.295	52.19±0.3733	9.327±0.1709	-	-	9.476±0.1709	9.571±0.0527	9.543±0.0060	-
1237671260664168763	0.04905±0.00001	-20.94±0.0036	0.4661±0.0048	2.537±0.0473	2.533±0.0412	0.8361±0.0730	0.8303±0.0629	49.71±0.5044	49.94±0.4551	10.43±0.0526	10.41±0.0093	10.35±0.0111	10.56±0.0526	10.63±0.0171	10.61±0.0032	10.55±0.0037
1237648720676061404	0.01658±0.00001	-19.43±0.0037	0.5734±0.0050	2.509±0.1272	2.593±0.0773	0.7942±0.1829	0.9298±0.1372	81.92±0.8638	81.72±0.7184	10.47±0.0959	9.985±0.0182	10.29±0.0093	10.60±0.09586	10.45±0.0403	9.960±0.0077	10.26±0.0040
1237650795680235542	0.01748±0.00001	-20.09±0.0034	0.7612±0.0046	2.425±0.0918	2.409±0.0666	0.6747±0.1040	0.6679±0.0742	75.58±0.4630	75.11±0.3188	10.82±0.0335	10.75±0.0065	10.70±0.0076	10.96±0.0335	10.81±0.0138	10.75±0.0028	10.70±0.0032
1237660763768029308	0.04594±0.00001	-20.60±0.0037	0.7064±0.0048	2.121±0.0302	2.244±0.0297	0.4453±0.0151	0.5188±0.0211	65.64±0.6157	63.91±0.5043	10.81±0.0476	10.83±0.0101	10.80±0.0108	10.96±0.0476	10.87±0.0183	10.88±0.0040	10.85±0.0043
1237648720676585591	0.05616±0.00001	-21.51±0.0041	0.5739±0.0053	1.909±0.1255	1.992±0.1411	0.3674±0.0323	0.3919±0.0475	48.93±0.6467	46.14±0.5125	11.04±0.0507	11.42±0.0157	11.26±0.0157	11.20±0.0507	11.27±0.0159	11.65±0.0050	11.49±0.0050
1237648720676585778	0.08781±0.00001	-22.37±0.0046	0.5505±0.0058	2.157±0.0395	2.254±0.0356	0.4640±0.0219	0.5264±0.0262	47.22±0.7476	47.54±0.5689	11.51±0.0415	11.31±0.0126	11.31±0.0126	11.66±0.0415	11.74±0.0130	11.54±0.0042	11.54±0.0042
1237665097926115359	0.01361±0.00001	-20.57±0.0035	0.7689±0.0048	2.833±0.1501	2.896±0.1480	1.502±0.4650	1.711±0.5267	71.60±0.3410	72.01±0.3140	11.17±0.0127	10.93±0.0901	11.26±0.0581	11.27±0.0127	11.18±0.0052	10.94±0.0364	11.27±0.0235
1237658493336879239	0.00683±0.00001	-18.15±0.0079	0.7368±0.0111	2.708±0.2508	2.744±0.2686	1.165±0.5845	1.252±0.6800	78.48±0.4699	77.49±0.4428	9.965±0.0465	-	-	10.08±0.0465	9.950±0.0193	10.41±0.0100	-
1237662890800000630	0.01268±0.00001	-18.50±0.0058	0.5313±0.0080	2.158±0.0306	2.225±0.0302	0.4645±0.0171	0.5062±0.0204	68.09±0.5463	67.65±0.5310	10.15±0.1015	9.785±0.0255	9.823±0.0278	10.30±0.1015	10.18±0.0399	9.818±0.0101	9.856±0.0110
1237658205573808201	0.01591±0.00001	-21.16±0.0036	0.5144±0.0051	2.323±0.0172	2.458±0.0302	0.5819±0.0152	0.7254±0.0381	62.33±0.3190	62.73±0.2845	10.74±0.0331	10.88±0.0326	10.50±0.0432	10.88±0.0331	10.81±0.0125	10.95±0.0123	10.57±0.0163
1237671122692210971	0.04662±0.00001	-20.73±0.0041	0.5637±0.0053	2.732±0.3064	2.995±0.3265	1.222±0.7550	2.101±1.434	86.29±1.977	85.16±1.097	11.05±0.0378	10.74±0.0334	10.56±0.0377	11.15±0.0378	11.02±0.0161	10.71±0.0142	10.53±0.0160
1237662890809983802	0.07255±0.00001	-19.72±0.0137	0.4970±0.0181	2.310±0.2028	2.340±0.3146	0.5705±0.1734	0.5974±0.2919	83.56	82.89	9.286±1.479	8.981±0.3235	10.31±0.0521	9.432±1.479	9.258±0.6236	8.954±0.1365	10.28±0.0223
1237667541753331904	0.02520±0.00002	-20.06±0.0061	0.7851±0.0082	2.596±0.1880	-	0.9346±0.3355	-	90	86.44±0.6861	11.28±0.0586	10.81±0.0819	10.24±0.1987	11.41±0.0586	11.24±0.0250	10.77±0.0349	10.21±0.0846
1237651800161321169	0.02127±0.00001	-20.56±0.0041	0.6593±0.0057	1.964±0.0016	2.061±0.0179	0.3829±0.0049	0.4176±0.0075	55.07±0.4327	56.74±0.4200	10.81±0.0522	10.70±0.0222	10.56±0.0270	10.97±0.0522	10.95±0.0184	10.83±0.0078	10.69±0.0095
1237667292659384635	0.02113±0.00001	-19.18±0.0045	0.4665±0.0061	2.542±0.1177	2.511±0.0799	0.8456±0.1844	0.7977±0.1156	79.50±0.6931	78.14±0.5597	10.15±0.1186	9.148±0.0740	9.909±0.0278	10.29±0.1186	10.14±0.0494	9.132±0.0308	9.892±0.0116
1237664667363246202	0.04422±0.00001	-21.83±0.0029	0.5348±0.0038	2.576±0.0757	2.635±0.0655	0.8998±0.1287	1.008±0.1285	53.40±0.4220	51.39±0.3650	11.41±0.0198	11.54±0.1565	11.28±0.1086	11.54±0.0198	11.58±0.0067	11.71±0.0527	11.45± 0.0366
1237667323784527982	0.05390±0.00001	-19.42±0.0085	0.3108±0.0122	2.075±0.1211	2.339±0.1569	0.4236±0.0527	0.5965±0.1452	88	87.71	11.13±0.1643	10.20±0.0346	10.22±0.0374	11.28±0.1643	11.09±0.0697	10.17±0.0149	10.18±0.0161
1237648720686415913	0.01847±0.00001	-21.09±0.0026	0.6883±0.0036	2.957±0.3331	3.004±0.2552	1.943±1.351	2.140±1.141	64.63±0.3169	64.37±0.2870	11.01±0.0142	11.06±0.0708	10.84±0.0603	11.09±0.0142	11.06±0.0055	11.11±0.0271	10.89±0.0231
1237648720152625168	0.02455±0.00001	-21.22±0.0030	0.5509±0.0041	2.096±0.0219	2.219±0.0199	0.4332±0.0102	0.5021±0.0132	60.19±0.3473	59.11±0.3164	11.51±0.0208	11.85±0.0940	11.53±0.0638	11.66±0.0208	11.60±0.0077	11.94±0.0345	11.62±0.0234
1237650760240005233	0.04583±0.00002	-21.32±0.0042	0.5275±0.0056	1.875±0.0228	1.942±0.0212	0.3591±0.0052	0.3762±0.0061	61.67±0.6592	59.59±0.5459	11.11±0.0517	10.94±0.0304	10.78±0.0426	11.26±0.0517	11.20±0.0191	11.02±0.0113	10.87±0.0158
1237661358615035950	0.00239±0.00002	-17.45±0.0350	0.5572±0.0495	2.561±0.0839	2.636±0.1070	0.8753±0.1377	1.009±0.2103	69.68±0.3021	69.31±0.3294	9.140±0.0797	-	-	9.272±0.0797	9.164±0.0317	9.219±0.0082	-
1237674648852627562	0.02076±0.00001	-20.66±0.0033	0.6051±0.0045	2.214±0.0167	2.309±0.0128	0.4986±0.011	0.5703±0.0103	51.83±0.3234	49.69±0.2642	10.71±0.0352	10.57±0.0083	10.43±0.0120	10.85±0.0352	10.89±0.0116	10.75±0.0028	10.62±0.0040
1237657856071827493	0.00327±0.00001	-16.70±0.0220	0.5093±0.0312	2.398±0.2538	2.488±0.1876	0.6562±0.2752	0.7657±0.2564	83.28±1.405	84.58±1.600	9.065±1.537	-	-	9.206±1.537	9.036±0.6488	9.648±0.0291	-
1237671140406657069	0.02839±0.00001	-21.34±0.0025	0.5328±0.0034	2.265±0.0301	2.237±0.0227	0.5348±0.0228	0.5144±0.0159	57.82±0.3197	58.58±0.3116	11.03±0.0338	11.26±0.0088	11.25±0.0090	11.18±0.0338	11.14±0.0122	11.37±0.0032	11.35±0.0033
1237650760778448980	0.01753±0.00001	-18.59±0.0069	0.4338±0.0086	2.146±0.1653	2.309±0.0628	0.4585±0.0891	0.5704±0.0537	90	90	10.64±0.2112	10.04±0.0335	10.08±0.0391	10.79±0.2112	10.60±0.0902	9.999±0.0144	10.05±0.0167
1237650760778449122	0.01720±0.00001	-16.85±0.0119	0.1541±0.0181	2.383±0.1947	2.189±0.1692	0.6401±0.2029	0.4832±0.1033	80.47±2.961	80.98	11.28±0.1826	8.576±0.3765	9.871±0.0406	11.43±0.1826	11.26±0.0766	8.554±0.1578	9.848±0.0173

SDSS DR16	z	M_g	$g-r$	$R50/R90_g$	$R50/R90_r$	n_g	n_r	i_g	i_r	$\mathbf{M_{KS}}$	$\mathbf{M_{KA}}$	$\mathbf{M_{KB}}$	$\mathbf{M_{nS}}$	$\mathbf{M_{IS}}$	$\mathbf{M_{IA}}$	$\mathbf{M_{IB}}$
1237650760241774845	0.05816±0.00002	-20.53±0.0070	0.4246±0.0096	1.866±0.0565	2.066±0.0645	0.3571±0.0126	0.4197±0.0273	57.98±1.2501	57.80±1.145	9.673±1.392	10.51±0.0764	10.71±0.0854	9.827±1.392	9.783±0.5006	10.62±0.0276	10.82±0.0308
1237650760241905743	0.07072±0.00001	-21.67±0.0040	0.6604±0.0052	2.384±0.0543	2.500±0.0445	0.6408±0.0567	0.7816±0.0626	67.82±0.6083	67.67±0.5337	11.30±0.0340	11.08±0.0203	11.01±0.0212	11.44±0.0340	11.33±0.0134	11.11±0.0081	11.05±0.0084
1237650760241905753	0.00525±0.00001	-15.32±0.0125	0.4579±0.0179	2.148±0.0569	2.165±0.6043	0.4594±0.0308	0.4687±0.3437	83.70±1.944	81.25±1.779	9.550±0.4342	-	-	9.702±0.4342	9.524±0.1828	8.988±0.0320	-
1237650760241971341	0.02725±0.00001	-20.12±0.0039	0.9143±0.0051	2.893±0.1370	2.940±0.1295	1.699±0.4836	1.874±0.5064	74.28±0.6195	75.71±0.4783	10.82±0.0287	10.17±0.0570	10.11±0.0591	10.92±0.0287	10.82±0.0118	10.17±0.0234	10.11±0.0243
1237650369407090853	0.02666±0.00001	-20.47±0.0036	0.6164±0.0049	2.677±0.2517	2.739±0.2183	1.093±0.5445	1.240±0.5465	75.61±0.4543	74.20±0.4063	11.05±0.0265	10.77±0.0347	10.56±0.0392	11.17±0.0265	11.05±0.0109	10.75±0.0144	10.56±0.0161
1237662195961686301	0.00235±0.00001	-17.46±0.0224	0.9756±0.0317	2.770±0.1235	2.813±0.1260	1.319±0.3316	1.440±0.3729	69.73±0.2837	70.08±0.2640	9.846±0.0207	-	-	9.959±0.0207	9.867±0.0083	9.790±0.0070	-
1237658491205582919	0.03519±0.00001	-19.89±0.0036	0.2614±0.0051	2.943±0.0662	2.961±0.1002	1.884±0.2603	1.960±0.4101	50.79±0.5725	54.07±0.5458	10.44±0.0978	10.08±0.0039	9.893±0.0076	10.53±0.0978	10.61±0.0329	10.25±0.0017	10.06±0.0028
1237655124470661181	0.02142±0.00001	-21.25±0.0029	0.6397±0.0041	2.817±0.0180	2.884±0.0170	1.451±0.0536	1.669±0.0589	26.20±0.2237	29.16±0.2206	10.81±0.0141	10.57±0.0116	10.50±0.0118	10.91±0.0141	11.44±0.0028	11.20±0.0023	11.13±0.0024
1237664291001335947	0.02366±0.00001	-20.74±0.0030	0.8766±0.0041	2.885±0.4705	2.799±0.3482	1.672±1.633	1.400±0.9990	78.06±0.1224	79.86±0.3336	11.25±0.0163	11.04±0.062	10.93±0.0524	11.36±0.0163	11.23±0.0068	11.02±0.0260	10.91±0.0219
1237661960790992019	0.06495±0.00001	-20.43±0.0073	0.5669±0.0091	2.341±0.1217	2.385±0.0757	0.5983±0.1132	0.6417±0.0791	79.60±1.900	77.95±1.437	10.92±0.0684	11.01±0.0146	10.97±0.0153	11.06±0.0684	10.90±0.0286	10.99±0.0065	10.95±0.0068
1237664289391116484	0.05087±0.00001	-19.42±0.0112	0.3271±0.0153	2.216±0.1163	2.301±0.1195	0.4996±0.0765	0.5632±0.0998	90	90	-	10.30±0.0389	10.25±0.0458	-	10.90	10.26±0.0169	10.21±0.0198
1237664289391182057	0.02569±0.00001	-18.66±0.0081	0.6199±0.0111	2.181±0.1209	2.316±0.0824	0.4778±0.0720	0.5757±0.0716	90	90	10.08±0.3785	10.41±0.0164	10.41±0.0190	10.23±0.3785	10.04±0.1620	10.37±0.0074	10.38±0.0085
1237661433771261955	-	-	-	-	-	-	-	63	63	-	-	-	-	-	-	-
1237648702966988820	0.01903±0.00001	-20.36±0.0040	0.6633±0.0055	2.397±0.0465	2.563±0.0589	0.6549±0.0503	0.8779±0.0970	57.11±0.3213	58.77±0.2956	10.46±0.0443	8.685±0.1248	10.21±0.0158	10.60±0.0443	10.57±0.0156	8.795±0.0449	10.32±0.0057
1237665441511964722	0.06461±0.00002	-21.28±0.0047	0.6358±0.0062	1.889±0.0933	1.988±0.3615	0.3622±0.0224	0.3906±0.1202	55.81±0.7264	56.79±0.5862	11.10±0.0492	11.12±0.0988	10.72±0.1129	11.26±0.0492	11.23±0.0174	11.25±0.0349	10.84±0.0399
1237661149765107752	0.01375±0.00001	-20.59±0.0034	0.7597±0.0048	2.297±0.0184	2.446±0.0424	0.5602±0.0152	0.7110±0.0521	63.95±0.2881	60.01±0.2838	10.86±0.0206	10.61±0.2320	10.19±0.1952	11.00±0.0206	10.93±0.0078	10.69±0.0870	10.26±0.0732
1237661971186188446	0.02387±0.00002	-19.09±0.0049	0.6643±0.0067	2.529±0.0695	2.581±0.0683	0.8249±0.1053	0.9080±0.1174	70.51±0.5996	70.39±0.5325	10.18±0.0595	10.17±0.0222	10.01±0.0274	10.31±0.0595	10.20±0.0238	10.19±0.0089	10.03±0.0110
1237667255627087966	0.05979±0.00001	-22.12±0.0030	0.7452±0.0040	2.367±0.0500	2.443±0.0431	0.6239±0.0499	0.7073±0.0524	52.71±0.4345	52.94±0.3619	11.55±0.0211	11.71±0.0989	11.59±0.0850	11.69±0.0211	11.71±0.0072	11.87±0.0335	11.76±0.0288
1237661970112577674	0.02538±0.00002	-19.13±0.0053	0.7827±0.0069	2.676±0.1554	2.743±0.1172	1.092±0.3357	1.249±0.2958	83.94±1.3636	83.20±0.8948	10.62±0.0509	10.36±0.0290	10.25±0.0350	10.74±0.0509	10.59±0.0215	10.33±0.0123	10.22±0.0148
1237651755087691887	0.04425±0.00001	-20.34±0.0042	0.4482±0.0057	2.328±0.0400	2.407±0.0452	0.5866±0.0360	0.6656±0.0501	74.47±0.7391	73.04±0.7846	10.32±0.0694	10.51±0.0091	10.42±0.0115	10.47±0.0694	10.32±0.0283	10.52±0.0039	10.43±0.0048
1237671764786020385	0.01072±0.00001	-19.66±0.0071	0.4213±0.0099	2.514±0.1591	2.895±0.6574	0.8020±0.2320	1.705±2.330	80.47±0.9116	76.33±0.5817	10.58±0.0748	10.49±0.0237	10.21±0.0409	10.70±0.0748	10.57±0.0311	10.47±0.0100	10.20±0.0171
1237671764786020514	0.02378±0.00002	-20.19±0.0046	0.4981±0.0063	1.874±0.0177	1.951±0.0191	0.3588±0.0041	0.3788±0.0056	42.38±0.5432	42.29±0.4694	10.43±0.1542	10.15±0.0507	9.873±0.0936	10.58±0.1542	10.73±0.0441	10.46±0.0145	10.18±0.0268
1237671764249477365	0.08212±0.00001	-22.34±0.0042	0.5488±0.0055	2.281±0.0780	2.475±0.0409	0.5465±0.0616	0.7485±0.0541	70.86±0.6026	72.44±0.5587	11.50±0.0371	11.24±0.0339	11.12±0.0350	11.64±0.0371	11.51±0.0150	11.25±0.0137	11.13±0.0141
1237648720698867721	0.00542±0.00001	-18.36±0.0119	0.4469±0.0160	2.018±0.0172	2.120±0.0247	0.4009±0.0063	0.4445±0.0123	58.35±0.5960	58.23±0.2713	9.535±0.1445	-	-	9.688±0.1445	9.642±0.0522	9.360±0.0156	-
1237671763175473314	0.02343±0.00002	-19.48±0.0053	0.6269±0.0073	2.439±0.1197	2.495±0.0992	0.7024±0.1441	0.7745±0.1377	90	90	10.36±0.1247	10.21±0.0283	10.17±0.0353	10.50±0.1247	10.33±0.0531	10.17±0.0121	10.13±0.0151
1237664289932640543	0.04725±0.00002	-18.97±0.0124	0.4851±0.0166	2.638±0.5595	2.519±0.2228	1.014±1.105	0.8097±0.3290	82.64	83.12	10.23±0.3040	10.56±0.0640	10.34±0.0831	10.36±0.3040	10.20±0.1281	10.54±0.0272	10.32±0.0352
1237648702972625038	0.02443±0.00002	-19.65±0.0054	0.7171±0.0073	2.212±0.0532	2.270±0.0395	0.4972±0.0346	0.5381±0.0302	59.57±0.8752	58.02±0.7076	10.45±0.0677	10.39±0.0536	9.995±0.0825	10.60±0.0677	10.55±0.0246	10.49±0.0195	10.10±0.0300
1237650761862086739	0.01342±0.00001	-17.81±0.0052	0.3517±0.0074	2.017±0.0436	2.325±0.1101	0.4006±0.0159	0.5839±0.0982	70.90±0.8044	68.82±0.8068	9.581±0.2929	8.968±0.0826	9.539±0.0415	9.731±0.2929	9.602±0.1168	8.989±0.0330	9.560±0.0166
1237650761862086708	-	-	-	-	-	0.00	2.00	65	65	-	-	-	-	-	-	-
1237671992947703853	0.02272±0.00001	-21.74±0.0027	0.7974±0.0038	2.166±0.5378	2.236±0.3851	0.4692±0.3066	0.5136±0.2685	60.64±0.3767	61.13±0.3292	11.55±0.0169	11.51±0.0603	11.44±0.0511	11.70±0.0169	11.63±0.0063	11.59±0.0224	11.53±0.0190
1237655499737661514	0.01435±0.00001	-20.79±0.0030	0.7145±0.0042	2.561±0.0404	2.672±0.0440	0.8754±0.0662	1.084±0.0943	63.71±0.3088	63.14±0.2797	10.45±0.0217	10.71±0.0224	10.38±0.0251	10.58±0.0217	10.51±0.0083	10.77±0.0085	10.45±0.0095
1237655499737727088	0.01328±0.00001	-20.77±0.0031	0.6695±0.0044	2.060±0.0622	2.158±0.0682	0.4173±0.0259	0.4649±0.0308	50.35±0.2961	47.05±0.2742	10.88±0.0188	8.780±0.3832	10.99±0.0236	11.04±0.0188	11.10±0.0060	8.994±0.1223	11.20±0.0076
1237662529524531258	-	-	-	-	-	-	-	57	57	-	-	-	-	-	-	-
1237662247667171600	0.02325±0.00001	-19.32±0.0047	0.6113±0.0062	2.243±0.0353	2.373±0.0829	0.5183±0.0251	0.6297±0.0840	80.52±1.003	81.63±0.9068	10.39±0.0737	10.20±0.0123	10.14±0.0164	10.54±0.0737	10.37±0.0309	10.18±0.0053	10.12±0.0069
1237667783917174819	0.02661±0.00001	-18.53±0.0056	0.4667±0.0077	2.585±0.2199	2.608±0.2781	0.9147±0.3819	0.9570±0.5114	77.41±1.284	76.68±1.210	9.849±0.2674	9.917±0.0183	9.934±0.0221	9.980±0.2674	9.837±0.1107	9.906±0.0078	9.922±0.0093
1237664291011887113	0.02334±0.00001	-21.40±0.0030	0.7781±0.0041	2.791±0.1435	2.919±0.1397	1.376±0.4041	1.795±0.5220	68.32±0.2687	68.12±0.2739	11.38±0.0161	11.23±0.0315	11.23±0.0278	11.49±0.0161	11.42±0.0064	11.26±0.0124	11.26±0.0110
1237662225686003729	0.01893±0.00001	-19.21±0.0036	0.6809±0.0049	3.097±0.2674	3.156±0.2571	2.599±1.449	2.943±1.572	64.69±0.4104	66.27±0.3846	10.24±0.0257	10.24±0.0081	10.16±0.0095	10.30±0.0259	10.29±0.0100	10.29±0.0032	10.21±0.0037
1237667783918026937	0.02774±0.00001	-20.92±0.0037	0.8519±0.0049	2.469±0.0355	2.619±0.0631	0.7399±0.0461	0.9778±0.1192	63.87±0.3889	59.69±0.3299	11.47±0.0229	11.12±0.0599	11.03±0.0560	11.61±0.0229	11.54±0.0086	11.19±0.0224	11.11±0.0210
1237654881271152801	0.00458±0.00002	-18.48±0.0169	0.3798±0.0239	2.439±0.0505	2.379±0.0107	0.7019±0.0608	0.6361±0.0110	81.83±1.064	73.08±0.3259	9.772±0.1239	-	-	9.915±0.1239	9.761±0.0513	9.961±0.0207	-
1237655495981990086	0.02454±0.00001	-20.76±0.0033	0.4636±0.0045	2.194±0.0403	2.079±0.0234	0.4860±0.0249	0.4254±0.0103	54.62±0.4411	54.59±0.4036	10.43±0.1114	10.75±0.0094	10.64±0.0115	10.58±0.1114	10.57±0.0386	10.90±0.0033	10.78±0.0040
1237662237477241008	0.01371±0.00001	-19.32±0.0062	0.6673±0.0087	2.480±0.1155	2.692±0.1946	0.7550±0.1547	1.129±0.4372	78.04±0.5975	78.02±0.4662	10.18±0.0817	9.553±0.0574	10.03±0.0264	10.31±0.0817	10.17±0.0339	9.539±0.0239	10.01±0.0110
1237662263240949953	0.01533±0.000004	-18.31±0.0044	0.2969±0.0063	2.525±0.1283	2.587±0.1073	0.8183±0.1922	0.9193±0.1875	90	90	-	12.25±0.1240	9.586±0.0268	-	10.17	12.21±0.0529	9.550±0.0115
1237674601605103640	0.02473±0.00001	-20.99±0.0029	0.5432±0.0040	1.991±0.0199	2.101±0.0214	0.3913±0.0067	0.4355±0.1006	48.66±0.3629	50.41±0.3331	10.92±0.0489	10.70±0.0063	10.67±0.0080	11.07±0.0489	11.12±0.0158	10.90±0.0022	10.87±0.0027
1237662224077815972	0.04270±0.00001	-21.38±0.0031	0.5834±0.0042	2.232±0.0332	2.380±0.0372	0.5109±0.0229	0.6371±0.0384	69.11±0.4350	70.21±0.3892	11.10±0.0299	10.70±0.0723	10.49±0.0780	11.25±0.0299	11.12±0.0119	10.72±0.0288	10.52±0.0311
1237648704054296626	0.00552±0.00001	-18.98±0.0101	0.3785±0.0143	2.407±0.1911	2.232±0.2775	0.6657±0.2119	0.5109±0.1914	42.73±0.5487	42.95±0.4785	9.882±0.1487	-	-	10.03±0.1487	10.18±0.0429	10.14±0.0049	-
1237662662133416147	0.02852±0.00001	-20.43±0.0035	0.5836±0.0047	2.326±0.0363	2.499±0.0799	0.5843±0.0324	0.7808±0.1123	59.69±0.3834	59.92±0.3610	10.65±0.0330	10.70±0.0595	10.29±0.0759	10.79±0.0330	10.74±0.0122	10.80±0.0218	10.39±0.0279
1237662224615342283	0.02889±0.00001	-19.21±0.0049	0.3347±0.0076	2.432±0.0528	2.508±0.0817	0.6942±0.0624	0.7946±0.1175	78.20±0.8934	78.03±0.8639	9.952±0.2726	8.793±0.1865	10.10±0.0346	10.09±0.2726	9.938±0.1133	8.779±0.0775	10.09±0.0144
1237674655289966817	0.05394±0.00002	-21.33±0.0040	0.6596±0.0052	2.162±0.0462	2.156±0.0307	0.4671±0.0260	0.4639±0.0170	64.61±0.5852	65.45±0.5084	11.00±0.0464	10.86±0.0320	10.75±0.0324	11.15±0.0464	11.05±0.0179	10.91±0.0124	10.80±0.0125
1237655498670211218	0.02380±0.00001	-21.30±0.0031	0.6246±0.0042	1.939±0.0125	1.958±0.0105	0.3755±0.0036	0.3809±0.0032	47.36±0.3902	47.79±0.3384	11.14±0.0257	11.06±0.0751	10.86±0.0690	11.29±0.0257	11.37±0.0081	11.29±0.0235	11.09±0.0216
1237648704056328322	0.00576±0.00001	-19.31±0.0145	1.082±0.0171	3.019±0.1780	3.179±0.2093	2.214±0.8235	3.086±1.339	59.86±1.717	71.52±0.2694	10.52±0.0153	-	-	10.58±0.0153	10.57±0.0067	10.25±0.0049	-
1237654881276395557	0.00548±0.00001	-18.35±0.0116	0.7032±0.0164	2.049±0.1103	2.129±0.0998	0.4131±0.0444	0.4495±0.0511	72.58±0.4457	72.57±0.3983	10.09±0.0430	-	-	10.25±0.0430	10.10±0.0174	9.988±0.0048	-
1237648704056918077	0.00554±0.00001	-19.54±0.0050	0.7909±0.0071	2.082±0.0139	2.177±0.0123	0.4271±0.0062	0.4756±0.0073	48.51±0.2785	47.46±0.2612	10.40±0.0164	-	-	10.55±0.0164	10.62±0.0052	10.82±0.0080	-
1237662305118650412	0.02942±0.00001	-21.54±0.0027	0.9078±0.0036	3.770±77.59	3.745±77.90	-	-	77.63±0.1778	75.29±0.3122	11.42±0.0153	11.57±0.0840	11.52±0.0695	11.13±0.0153	11.42±0.0064	11.56±0.0347	11.51±0.0287
1237667781239636022	0.03746±0.00001	-21.94±0.0023	0.7166±0.0032	3.028±0.2211	3.178±0.2155	2.255±1,041	3.079±1.376	67.19±0.2664	68.15±0.2879	11.45±0.0124	11.62±0.0912	11.45±0.0714	11.50±0.0124	11.48±0.0049	11.65±0.0358	11.49±0.0280
1237668272980754643	0.04618±0.00001	-18.61±0.0136	0.5679±0.0179	2.384±0.1645	2.515±0.1536	0.6408±0.1716	0.8035±0.2245	88.37	84.41	10.96±0.1383	9.056±0.2834	10.20±0.0626	11.10±0.1383	10.93±0.0587	9.024±0.1201	10.17±0.0268
1237651736313528355	0.00449±0.00001	-19.17±0.0068	0.8389±0.00955	2.395±0.0430	2.485±0.0580	0.6527±0.0463	0.7615±0.0787	59.23±0.3147	59.17±0.3066	10.35±0.0166	-	-	10.49±0.0166	10.45±0.0061	10.53±0.0140	-
1237661211510833280	0.01731±0.00001	-18.64±0.0048	0.3216±0.0068	2.417±0.1768	2.589±0.2598	0.6762±0.2009	0.9224±0.4559	90	90	9.732±0.9970	8.830±0.1739	10.10±0.0388	9.869±0.9970	9.688±0.4283	8.786±0.0747	10.06±0.0167
1237655692481986636	0.00931±0.00002	-18.98±0.0087	0.6012±0.0123	2.375±0.2090	2.584±0.2332	0.6315±0.2130	0.9144±0.4046	55.15±0.3791	59.30±0.3398	10.00±0.0813	-	-	10.14±0.0813	10.12±0.0290	9.833±0.0088	-
1237655550742298700	0.03065±0.00001	-21.51±0.0027	0.7833±0.0036	2.903±0.1762	3.065±0.1529	1.734±0.6356	2.434±0.7770	64.43±0.4319	64.49±0.3343	11.53±0.0118	-	-	11.62±0.0118	11.59±0.0046	11.33±0.0182	-
1237662302453039177	0.03107±0.00001	-21.40±0.0029	0.6500±0.0039	2.938±0.4964	3.141±0.4087	1.866±1.932	2.850±2.422	74.82±0.4532	73.73±0.3613	11.35±0.0176	10.75±0.0734	10.62±0.0765	11.42±0.0176	11.35±0.0072	10.75±0.0300	10.62±0.0313
1237654954281468455	0.02745±0.00002	-20.90±0.0038	0.7251±0.0052	2.151±0.0307	2.314±0.0265	0.4608±0.0167	0.5742±0.0229	64.56±0.4135	66.58±0.3806	10.93±0.0473	10.77±0.0264	10.61±0.0310	11.08±0.0473	10.98±0.0183	10.81±0.0102	10.65±0.0120
1237652598487646631	0.02009±0.00001	-19.87±0.0044	0.8528±0.0057	2.898±0.3517	2.931±0.2473	1.719±1.257	1.840±0.9486	80.25±0.7415	86.53±1.107	10.91±0.0307	10.62±0.0303	10.11±0.0609	11.01±0.0307	10.89±0.0130	10.60±0.0128	10.08±0.0257
1237656567038935144	0.01263±0.00001	-19.95±0.0046	0.7910±0.0064	2.174±0.3360	2.353±0.1881	0.4739±0.1962	0.6101±0.1809	53.13±0.3387	53.74±0.2710	10.58±0.0239	8.496±0.8907	10.42±0.0627	10.73±0.0239	10.74±0.0082	8.653±0.3038	10.58±0.0214
1237652944768008329	0.01672±0.00001	-19.92±0.0035	0.6668±0.0048	2.664±0.0298	2.713±0.0235	1.066±0.0626	1.175±0.0552	57.05±0.3627	53.50±0.3082	10.51±0.0263	8.438±0.0008	10.47±0.0104	10.64±0.0263	10.65±0.0092	8.574±0.0008	10.61±0.0037
1237663457240089137	0.02044±0.00001	-20.13±0.0042	0.4531±0.0059	2.290±0.03078	2.254±0.0231	0.5544±0.0250	0.5262±0.0170	60.29±0.3979	59.92±0.3734	10.15±0.0794	10.14±0.0160	10.11±0.0191	10.29±0.0794	10.24±0.0292	10.23±0.0059	10.20±0.0071
1237663456703545733	0.01929±0.00001	-20.73±0.0035	0.7256±0.0048	1.959±0.2705	2.072±0.2610	0.3814±0.0821	0.4225±0.1127	53.36±0.3495	55.40±0.3161	10.80±0.0269	10.74±0.0660	10.24±0.0950	10.95±0.0269	10.95±0.0093	10.88±0.0228	10.39±0.0328
1237666210347614532	0.05536±0.00001	-20.13±0.0061	0.5283±0.0081	2.477±0.1513	2.569±0.1622	0.7501±0.2007	0.8889±0.2714	87.43	55	10.96±0.0604	11.32±0.0060	11.29±0.0058	11.10±0.0604	10.93±0.0257	11.29±.0030	11.26±0.0030
1237666210347745660	0.01756±0.00002	-19.76±0.0059	0.4868±0.0081	2.242±0.0344	2.300±0.0368	0.51793±0.0244	0.5627±0.0307	71.25±0.5229	71.30±0.4510	10.15±0.1237	8.825±0.2138	9.884±0.0560	10.30±0.1237	10.17±0.0498	8.839±0.0860	9.898±0.0225
1237663543150837809	0.01616±0.00001	-21.20±0.0024	0.8060±0.0034	3.360±0.1321	3.304±0.1188	4.474±1.1978	3.995±0.9695	49.48±0.2253	48.93±0.2189	10.85±0.0115	10.56±0.0264	10.53±0.0257	10.83±0.0115	11.06±0.0037	10.77±0.0085	10.73±0.0083
1237663784191524949	0.02489±0.000001	- 20.85±0.0070	0.4298±0.0103	1.980±0.1884	2.033±0.3359	0.3880±0.0611	0.4064±0.1284	60.26±0.6040	61.58±0.5911	10.43±0.0991	10.38±0.0161	10.32±0.0199	10.58±0.0991	10.51±0.0368	10.46±0.0060	10.40±0.0075
1237672815977496655	-	-	-	-	-	-	-	81	81	-	-	-	-	-	-	-
1237669518514913516	-	-	-	-	-	-	-	60	60	-	-	-	-	-	-	-

Table A2. Dynamical masses of a subsample of 145 LTGs from Catinella et al. (2005) with photometric and/or spectroscopic information in the SDSS DR16.

AGC Name	Other Name	SDSS DR16 Name	α J2000	δ J2000	$\mathbf{M_{Dyn}}$ $10^{11}\mathbf{M_{solar}}$
144	456-044	1237653653447180545	00 15 26.8	16 14 05	0.61±0.17
400814	-	1237652629638873182	00 31 56.7	-10 15 08	3.05±0.51
400343	N217	1237652947456360495	00 41 33.7	-10 01 18	6.51± 1.06
400373	M-203006	1237652947993624616	00 45 08.8	-09 37 53	0.46±0.15
400846	M-203014	1237652900753244294	00 47 25.2	-09 51 10	0.27±0.07
400390	M-203015	1237652900753244175	00 47 46.2	-09 50 05	2.46±0.48
400387	UA14	1237652900753244328	00 47 46.5	-09 53 54	0.06±0.02
400848	-	1237652947993952343	00 47 51.9	-09 38 46	0.23±0.05
410518	384-064	1237663782593822774	01 04 15.0	-01 06 51	0.58±0.23
410526	-	1237666338115027075	01 04 41.5	00 57 24	0.29±0.05
410530	-	1237663783130759334	01 04 51.7	00 38 52	0.19±0.07
410531	-	1237666338115092762	01 04 58.0	00 50 59	2.34±0.69
410534	-	1237663783130824820	01 05 26.2	00 48 07	1.85±0.49
410541	M+004027	1237666338652618892	01 11 15.8	00 27 21	0.15±0.04
410770	A168-33	1237663784205680908	01 15 51.2	00 08 48	1.84±0.70
866	385-072	1237666339190472839	01 20 06.6	00 12 20	0.08±0.03
894	I1681	1237663784206270641	01 21 21.2	00 05 24	0.10±0.03
915	N497	1237666338116993064	01 22 23.8	00 52 32	16.18±2.68
931	385-094	1237663783132790881	01 23 14.5	00 42 04	0.03±0.01
410148	385-093	1237657189840584856	01 23 17.0	00 54 22	0.70±0.17
1116	386-007	1237663782597034125	01 33 34.5	-01 05 27	0.39±0.12
1120	386-010	1237663782597099527	01 34 02.4	-01 04 33	1.21±0.23
1123	386-011	1237657069546831898	01 34 08.0	-01 01 58	1.16±0.26
410955	-	1237678880495894618	01 50 54.7	-02 22 23	0.91±0.31
1428	I1755	1237653652921057594	01 57 09.8	14 32 59	2.43±0.74
410408	N747	1237652900223909957	01 57 30.2	-09 27 45	0.79±0.16
1901	N926	1237663783676477669	02 26 06.6	00 19 55	6.52±1.57
420405	-	1237657070628503722	02 47 00.2	00 09 20	2.77±0.91
420434	-	1237657584951034038	02 48 34.2	00 59 33	0.88±0.17
2291	I1856	1237663783142096968	02 48 50.7	00 46 02	2.56±0.72
420384	389-026	1237663783142228130	02 49 35.2	00 43 25	0.52±0.15
420428	-	1237663783142228165	02 49 49.2	00 47 35	2.56±0.83
2319	389-029	1237657584951230617	02 49 53.5	-01 00 13	2.54±0.42
420308	N1148	1237652900767268885	02 57 04.0	-07 41 08	0.75±0.15
2479	M+008065	1237663784217149628	03 00 40.2	00 01 13	0.47±0.15
2628	390-041	1237666300018229273	03 16 31.7	00 28 07	2.09±0.33
430240	N1324	1237649964066406405	03 25 01.6	-05 44 42	11.32±1.74
3917	N2410	1237653588477411643	07 35 02.4	32 49 20	6.87±1.09
4257	118-069	1237660764834103400	08 10 11.1	24 53 32	0.91±0.25
4308	119-029	1237664837535858925	08 17 25.8	21 41 07	0.84±0.24
180814	-	1237667782809223472	08 18 24.8	11 37 08	0.19±0.07
180815	-	1237667782809223502	08 18 27.7	11 37 52	1.82±0.58

AGC Name	Other Name	SDSS DR16 Name	α J2000	δ J2000	$\mathbf{M_{Dyn}}$ $10^{11}\mathbf{M_{solar}}$
180869	-	1237661086957568117	08 27 13.3	25 58 01	3.80±0.91
4501	N2620	1237664092898852896	08 37 28.2	24 56 47	11.74±1.93
4691	N2713	1237654601019686930	08 57 20.6	02 55 14	19.48±3.57
4698	150-053	1237664093438214204	08 58 32.5	28 15 59	11.81±2.00
4823	N2777	1237660412649865229	09 10 41.7	07 12 23	0.14±0.05
190864	-	1237671260664168763	09 15 28.2	11 50 05	0.15±0.05
4915	006-026	1237648720676061404	09 17 29.0	00 37 14	0.95±0.25
4923	I531	1237650795680235542	09 17 50.5	00 16 44	1.22±0.30
190809	-	1237660763768029308	09 18 33.4	34 20 42	1.67±0.64
490302	-	1237648720676585591	09 22 09.6	00 32 22	05.02±1.33
490303	-	1237648720676585778	09 22 22.6	00 29 18	5.26±1.22
5010	N2862	1237665097926115359	09 24 55.2	26 46 29	5.14±1.25
5064	I540	1237658493336879239	09 30 10.1	07 54 07	0.22±0.07
190788	092-049	1237668289080000630	09 46 30.7	15 53 09	0.33±0.08
5250	N2998	1237658205573808201	09 48 43.5	44 04 50	3.46±0.81
190867	-	1237671122692210971	09 49 53.4	12 54 35	3.53±1.27
191921	-	1237668289080983802	09 56 06.9	16 17 22	0.32±0.09
5341	123-008	1237667541753331904	09 56 35.9	20 38 41	14.9±2.19
5472	I594	1237651800161321169	10 08 32.0	00 40 02	1.32±0.23
201117	-	1237667292659384635	10 21 34.5	23 57 34	0.51±0.12
5813	184-004	1237664667363246202	10 41 08.8	36 22 20	9.19±1.59
201196	-	1237667323784527982	10 44 05.6	26 03 41	0.27±0.09
5985	I653	1237648720686415913	10 52 06.8	00 33 39	2.85±0.53
6340	011-059	1237648720152625168	11 19 55.2	00 52 45	6.30±1.28
510263	012-002	1237650760240005233	11 31 38.0	-03 38 51	3.23±0.73
6595	N3769	1237661358615035950	11 37 44.0	47 53 34	0.15±0.04
6608	012-046	1237674648852627562	11 38 33.2	-01 11 04	1.91±0.36
6667	268-071	1237657856071827493	11 42 25.2	51 35 50	0.08±0.02
6720	I728	1237671140406657069	11 44 50.4	-01 36 05	2.10±0.34
510217	012-079	1237650760778448980	11 46 16.8	-03 10 50	0.64±0.15
510383	-	1237650760778449122	11 46 33.2	-03 08 25	0.08±0.03
510381	-	1237650760241774845	11 48 01.7	-03 42 25	1.01±0.21
510373	-	1237650760241905743	11 49 09.6	-03 37 08	2.44±0.53
510377	-	1237650760241905753	11 49 12.6	-03 39 35	0.10±0.03
510161	012-097	1237650760241971341	11 49 37.9	-03 34 07	2.76±0.53
510306	012-100	1237650369407090853	11 49 49.7	-03 31 03	1.41±0.24
6973	I750	1237662195061686301	11 58 51.9	42 43 20	0.22±0.04
211853	-	1237658491205582919	11 59 50.9	08 47 35	0.20±0.06
7015	N4043	1237655124470661181	12 02 23.0	04 19 47	0.23±0.07
7196	098-095	1237664291001335947	12 11 59.2	15 24 03	7.22±1.72
221736	-	1237661950790992019	12 15 49.2	13 11 48	1.25±0.37
221829	-	1237664289391116484	12 16 03.2	14 00 46	0.55±0.19
221828	FGC1395	1237664289391182057	12 16 11.6	13 59 34	1.15 ±0.42

AGC Name	Other Name	SDSS DR16 Name	α J2000	δ J2000	$\mathbf{M_{Dyn}}$ $10^{11}\mathbf{M_{solar}}$
7297	N4226	1237661433771261955	12 16 26.2	47 01 32	2.52±0.56
7337	013-121	1237648702966988820	12 18 08.6	-01 03 52	0.91±0.16
221991	-	1237665441511964722	12 19 44.0	29 34 49	1.85±0.48
7478	N4357	1237661149765107752	12 23 58.7	48 46 45	3.67±0.81
221659	-	1237661971186188446	12 25 41.7	07 10 01	0.28±0.09
221928	-	1237667255627087966	12 26 51.7	31 05 39	6.11±1.75
222003	-	1237661970112577674	12 27 06.5	06 25 32	0.56±0.15
221950	-	1237651755087691887	12 32 59.7	03 23 37	1.05±0.32
7883	015-002	1237671764786020385	12 42 57.2	-01 13 46	0.90±0.19
520620	015-003	1237671764786020514	12 43 02.9	-01 16 58	0.70±0.14
520563	-	1237671764249477365	12 44 52.0	00 25 48	6.52±1.55
7931	N4668	1237648720698867721	12 45 31.7	00 32 09	0.09±0.02
7963	015-022	1237671763175473314	12 47 52.7	-01 11 10	1.33±0.22
222035	-	1237664289932640543	12 59 44.2	14 10 54	1.67±0.50
8238	016-013	1237648702972625038	13 09 41.0	-01 02 53	1.99±0.36
530631	-	1237650761862086739	13 16 34.0	-02 17 22	0.08±0.03
8348	I4218	1237650761862086708	13 17 03.4	-02 15 40	2.15±0.40
8475	N5174	1237671992947703853	13 29 25.7	11 00 28	7.45±1.51
8485	N5183	1237655499737661514	13 30 06.1	-01 43 13	1.93±0.44
8487	N5184	1237655499737727088	13 30 11.5	-01 39 47	3.35±0.51
8518	N5207	1237662529524531258	13 32 14.0	13 53 31	7.46±1.36
231092	045-042	1237662247667171600	13 36 35.5	08 11 34	0.74±0.25
231195	-	1237667783917174819	13 45 36.9	22 03 16	0.32±0.08
8766	I944	1237664291011887113	13 51 30.8	14 05 30	10.12±2.05
231174	-	1237662225686003729	13 52 21.2	38 11 43	0.17±0.05
8828	132-040	1237667783918026937	13 54 26.7	21 49 45	3.27±1.04
8831	N5356	1237654881271152801	13 54 58.4	05 20 00	0.39±0.07
8844	018-004	1237655495981990086	13 55 59.4	-01 15 42	2.32±0.41
8918	074-031	1237662237477241008	14 00 14.5	08 58 01	0.33±0.07
230925	074-035	1237662263240949953	14 00 31.0	08 39 01	0.25±0.06
8994	018-042	1237674601605103640	14 04 52.5	00 36 39	1.02±0.23
241267	M+631092	1237662224077815972	14 17 11.6	35 24 30	2.87±0.64
9201	N5584	1237648704054296626	14 22 23.7	00 23 18	1.37±0.29
241270	M+632024	1237662662133416147	14 24 12.0	35 08 45	0.6±0.13
241336	-	1237662224615342283	14 24 58.2	35 21 15	0.80±0.22
540242	019-024	1237674655289966817	14 25 49.7	-02 20 01	5.45±1.16
9250	N5618	1237655498670211218	14 27 11.8	-02 15 46	1.36±0.26
9462	N5719	1237648704056328322	14 40 56.0	00 19 04	0.72±0.10
9483	I1048	1237654881276395557	14 42 57.9	04 53 24	0.52±0.12
9512	N5750	1237648704056918077	14 46 11.1	00 13 22	0.73±0.13
9537	193-001	1237662305118650412	14 48 26.7	34 59 50	4.56±0.79
9538	I1058	1237667781239636022	14 49 12.3	17 01 13	2.82±0.73
241306	-	1237668272980754643	14 51 18.7	16 41 41	0.64±0.21

AGC Name	Other Name	SDSS DR16 Name	α J2000	δ J2000	$\mathbf{M_{Dyn}}$ $10^{11}\mathbf{M_{solar}}$
9645	N5806	1237651736313528355	15 00 00.3	01 53 28	1.01±0.22
9681	M+731023	1237661211510833280	15 03 39.7	42 07 33	0.32±0.07
9888	I1125	1237655692481986636	15 33 05.6	-01 37 42	0.22±0.05
10306	023-031	1237655550742298700	16 16 43.5	00 14 46	10.15±1.52
10692	139-034	1237662302453039177	17 05 28.0	23 09 11	4.76±0.73
10706	197-035	1237654954281468455	17 06 28.3	38 21 47	1.83±0.30
600138	M-153012	1237652598487646631	20 49 52.0	-07 01 17	4.41±0.75
11649	374-028	1237656567038935144	20 55 27.6	-01 13 31	1.44±0.34
310030	426-015	1237652944768008329	21 12 01.2	11 29 45	0.20±0.05
610024	375-011	1237663457240089137	21 13 12.8	00 21 58	0.86±0.15
11712	N7047	1237663456703545733	21 16 27.6	00 49 36	2.28±0.49
610495	-	1237666210347614532	21 56 49.5	-07 45 33	1.45±0.45
610499	-	1237666210347745660	21 58 05.8	-07 50 43	0.73±0.16
12174	N7364	1237663543150837809	22 44 24.2	00 09 44	2.58±0.39
12363	379-034	1237663784191524949	23 06 31.5	00 10 18	0.99±0.20
35971	604G7	1237672815977496655	23 15 17.2	-21 21 57	3.18±0.85
12834	N7782	1237669518514913516	23 53 54.0	07 58 14	9.73±1.59

This paper has been typeset from a TEX/LATEX file prepared by the author.